From Knowledge to Wisdom

JSOE

Journal of Shipping and Ocean Engineering

Journal of Shipping and Ocean Engineering

Journal of Shipping and Ocean Engineering

Volume 4, Number 1-2, February 2014 (Serial Number 11)

Contents

Ship Technology

Ship Industry

Chemical Oceanography

Geological Oceanography

Interaction of Ships within Navigable Ice Channel

Vadim K. Goncharov[1, 2], Natalia Yu. Klementieva[1, 3] and Kirill E. Sazonov[3]

1. Department of Ocean Technique and Marine Technologies, Saint-Petersburg State Marine Technical University, Saint-Petersburg 190008, Russia

2. Department of Engineering Environmental Protection, Saint-Petersburg State Electrotechnical University, Saint-Petersburg 197376, Russia

3. Ice Laboratory, Krylov State Research Centre, Saint-Petersburg 196158, Russia

Abstract: At intensive winter navigation, the ships should separate under movement on opposite courses or make overtaking of slowly moving cargo vessels in the water areas covered with ice. Under navigation within ice channel, possibilities for maneuvering are reduced; therefore, danger of collision of ships exists. The ice floes between vessels hulls and outside are the major factors defining values and direction of side force and yawing moment that arise on their hulls during divergence. Ice loads on the ship hull exceed considerably the loads caused by water flow around hull. Performed previously experiments in the ice basin have detected that besides increase of side force and yawing moment modules the change of side force directions occurs during the divergence of vessels in comparison with same maneuvering on water area without ice cover. Article contains the detailed problem definition and mathematical model of ships interaction during opposite passing by or overtaking and technical approach to computation of loads on vessels hulls. As example of strategy application, the simulation of loads on overtaking ship was performed, and main results of computations are presented. Outcomes of investigation are character of variation of side force and yawing moment during passage along overtaken ship and dependence of the peak values of additional ice resistance, side force and yawing moment on beam distance between vessels and thickness that are contained in the article.

Key words: Ship, ice channel, ice concentration, navigation, overtaking, opposing traffic, side force, yawing moment.

1. Introduction

One of the principal methods of winter navigation is motion of ships within the navigable ice channel [1]. Ice channel is made and then maintained improper condition for navigation by icebreakers. This variant of winter navigation was previously used mainly in approaches to ports situated in Arctic seas. Currently, navigable ice canals have become principal lanes for navigation in the eastern part of the Gulf of Finland during winter and spring time.

Within the navigable ice channel, on-coming motion and overtaking vessels take place at a slow speed. Such maneuvers are performed in the area limited with channel borders; therefore, there is

possible danger of collision in case of inadequate performance mutual maneuvering.

It is commonly known that in case of close approach situation in water area free of ice, there is hydrodynamic interaction between vessels' hulls, which causes at the side force and yawing moment to appear. These effects result from narrowing water area between hulls owing to which speeds of the current in the area between the hulls become greater than on the other sides of hulls. As a result, athwart ship force-side force directed to the area between the vessels and yawing moment result capable to cause collision in case of inadequate maneuvering.

The effects appearing in case of close approach situation in free water area are thoroughly studied both theoretically and experimentally [2, 3]. On base of its outcomes, the instructions on performing safe maneuvering, which are used in initial and further

---

Corresponding author: Vadim K. Goncharov, doctor of eng., professor, research fields: bubbles and drops dynamics, ice mechanics, safety of winter navigation and environment effect of oil and gas transportation. E-mail: vkgonch@mail.ru.

training of deck officers including skill training of maneuvering on navigational simulator, have been developed.

When navigating ship in ice conditions, the main part of loads on the hull is connected with ice cover of sea. Energies consumed for breaking ice cover, turning and moving formed ice floes athwart hull, and under the hull as well as ice friction against plating of hull determine ice propulsion qualities of the vessels. Importance of interaction of hull with water mass is not considerable and therefore, not taken into account in practical evaluations of ice propulsion qualities of ships [4, 5].

This allows expecting that when maneuvering in case of close approach situation, the forces caused by interaction of the vessels hulls with ice will prevail as well. Therefore, the nature of vessels hulls interaction in ice condition will considerably differ from such interaction when there is no ice cover. Consequently, control of vessels traffic when maneuvering in ice conditions should significantly differ from control in open waters. Therefore, vessels interaction research when proceeding in ice channel is of great practical interest and results of this research will be a ground for assessment of safe distance between vessels when maneuvering as well as for developing navigational simulators in reference with vessel proceeding in navigable ice channel.

To research the effects appearing when on-coming and overtaking vessels in navigable ice channel, special experiments were carried out in the ice towing tank. Results of the experiments, described in Ref. [6, 7] showed that vessels hulls interaction in ice conditions does considerably differ from hulls interaction in case of water area free of ice.

First, differences appear in the fact that variation of side force, ice resistance and yawing moment in passing-by process contains pulse components of significant value, which can be compared to average values of these parameters. The described pulses were explained by hull interactions with separate ice floes

getting between hulls of the vessels.

Analysis of average values of side force and yawing moment variation when passing has shown that:

• Side force is directed to the opposite side relative to overtaken or overtaking vessel (i.e., sign is changed to the opposite in respect with water area free of ice);

• Yawing moment does not change sign (direction) in passing by process.

Experiments, discovered considerable difference in nature of vessels interaction in ice channel from interaction in water area free of ice, determined importance of special theoretical researches for the purpose of parameterization and explaining the observed effects.

The first results of theoretical assessment were briefly described in the Ref. [6, 7]. In this article, the considered problem, advanced mathematical model, data of numerical modeling of overturning in navigable ice channel, and assessment of obtained results are given in details.

2. Description of the Problem

Navigable ice channel is the remained after icebreaker passage canal filled with not large ice floes and ice brush, which were formed as a result breaking ice cover with icebreaker hull and crushing separate ice floes with propeller screws [1]. First, after forming the channel (fresh channel), it represents open water lane limited with compact ice pack or fast ice and partly filled with ice floes. (Channel scheme on initial stage is given in Fig. 1a). Then, freezing over on the open water surface of the channel and freezing of separate ice floes filling the canal take place. This ice cover of the channel is broken by the vessels proceeding along the canal, and gradually water areas free of ice disappear, and the channel becomes filled with ice brush (old channel). (Channel scheme on final stage is given in Fig. 1b). Layer thickness of freezing ice brush in the channel begins to exceed compact ice thickness outside the channel, proceeding of vessels along the channel becomes impossible, and
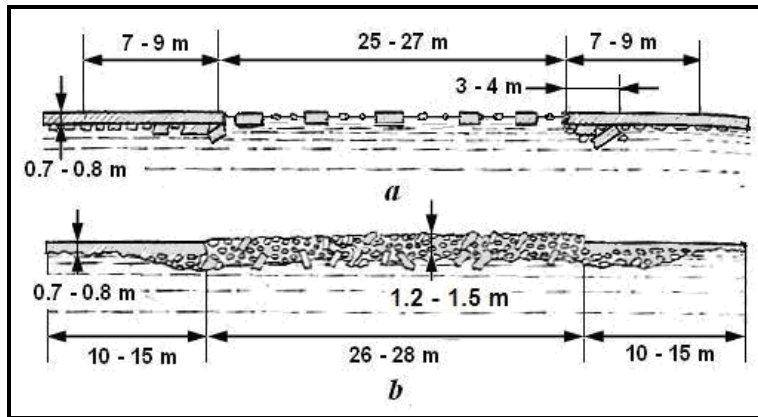
Fig. 1 Schema of the navigable ice channel (a) after creation by icebreaker and (b) at last stage of its using for traffic.

new channel is formed in parallel to the old one filled with frozen ice brush.

Vessels maneuvering (oncoming passing and overtaking), when proceeding along the ice, channel is limited with its borders and complicated by ice floes filling the channel. Ice impact on the vessel hull in the channel is realized in ice resistance, which depends on ice thickness and its concentration. Ice concentration in the channel is greater incase if there are vessels in it in comparison with the canal free of vessels. Such effect causes ice resistance variation when vessel maneuvering (passing by) and appearing side force as well as yawing moment on the vessel hull. The given research describes vessel navigation in ice canal on its initial stage.

Ice brush filling navigable ice channel can be characterized using the following parameters: average transverse ice floe size–b_{Ice}, its thickness–h_{Ice} and concentration–s. Observation of the ice canals formed by ice-breakers [8] showed that multiplying value ($b_{Ice} \cdot h_{Ice}$) is relatively constant and is connected with the ice cover thickness h. Such connection can be represented with the following empirical equation:

$$b_{Ice} = 0.54 h_{Ice} + 0.45 \qquad (1)$$

When vessel gets into the channel, her hull pushes separate ice floes aside to the borders, causing increase of ice concentration in the area between sides of the vessel and borders of the channel in comparison with initial concentration S_0, as it is shown in Fig. 2.

If a vessel proceeds not strictly along the channel, ice concentration at her starboard side which is closer to the canal border s_2, becomes greater than at the opposite port side s_1, that is $s_2 > s_1 > s_0$. As ice resistance to motion increases with ice concentration, ice resistance at starboard side R_s gets greater than port side resistance R_l, that is $R_s > R_l$. As a result yawing moment M_{yaw} appears, which is directed to starboard relative to amidships as it is shown in Fig. 3.

In case of two vessels, on-coming passing by or overtaking similar effect takes place: ice concentration along the first vessel hull from the side of on-coming or overtaken second vessel increases additionally relative to ice concentration before closing situation. Ice concentration between vessels hulls increases inversely to beam distance between vessels hulls–d,
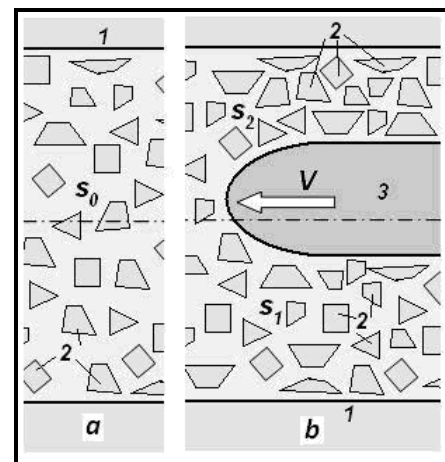
Fig. 2 Variation of ice concentration within navigable ice channel under vessel motion. Notation: _1_–border of channel, _2_–ice floes (broken ice), _3_–vessel.
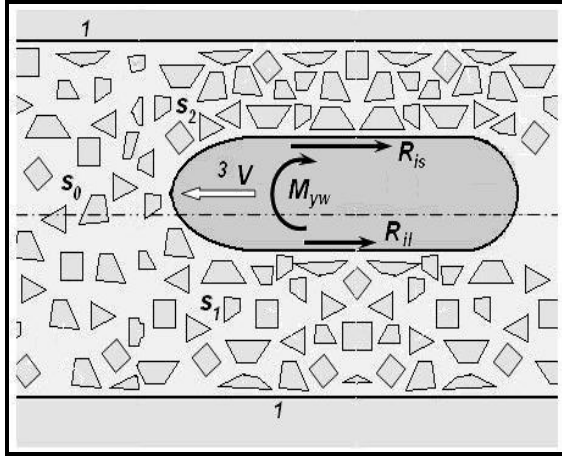
Fig. 3 Yawing moment M_{yw} arising under vessel motion near ice channel border.

causing side force and yawing moment directed to on-coming vessel to appear.

For the purpose of vessels interaction research, it is reasonable to model this effect replacing on-coming or overtaken vessel with sudden narrowing borders of ice canal as it is shown in Fig. 4., In this case, initial distance from vessel starboard side to channel border do is reduced to the value d, which is the function of mutual position of vessels, and then is recovered after vessels passing. Speed of the given vessel incase of on-coming passing of the model is equal to the sum of both vessels speeds $V_1 + V_2$. Casing of overtaking of slowly moving vessel, the speed of the given vessel is equal to deduction of both vessels speeds V_1-V_2. To assess side force and yawing moment appearing when passing by vessels, ice impact on the vessel hull along each side correspondingly varying ice concentration

should be parameterized, and then integration of longitudinal and transversal component of ice load.

During vessels passing by, ice concentration and ice resistance variation take place only at the side directed to the second vessel. The effects caused by this change initial side force and yawing moment, which affected the vessel prior to getting close to the second vessel. As vessel control was adapted to such conditions, just these effects appearing when vessels passing by are of great practical interest. This allows investigating vessel interaction without considering channel borders impact that is in continuous ice brush field with varying concentration s and ice floes thickness h_{Ice}. It is supposed, that in case of passing by vessels maintain their speed and mutual path of motion.

When motion in broken ice with concentration of less than 10 balls, vessel takes up separate ice floes impacts, which are shown by pulse components in ice resistance and appearing alternating variation (relative to average) side force and yawing moment, as it was proved by modeling experiments [6, 7]. These effects were not described in the given research. Besides, side force and yawing moment of hydrodynamic nature on the vessel hull appearing in case of close approach situation were not taken into consideration as well, as ice loads to hull prevail in ice condition.

Further, solution of the problem as to increasing of ice resistance, appearing side force and yawing moment of the vessel overtaking another vessel motion at a relatively slower speed is developed.

Fig. 4   Simulation of opposite motion of two vessels by means of local constriction of ice channel.

3. Definition of Mathematical Model of Ships Interaction

Kinematic scheme of the task is shown in Figs. 5a and 5b. Two systems of axes are used. The first system of axes $\xi O \zeta$ is stationary; it is connected with the stern of overtaken vessel «2» with length L_2, which is supposed to be motionless. The second system of axes xOy is mobile, it is connected with the bow of overtaking vessel «1» with length L_1, which proceeds at a speed equal to disc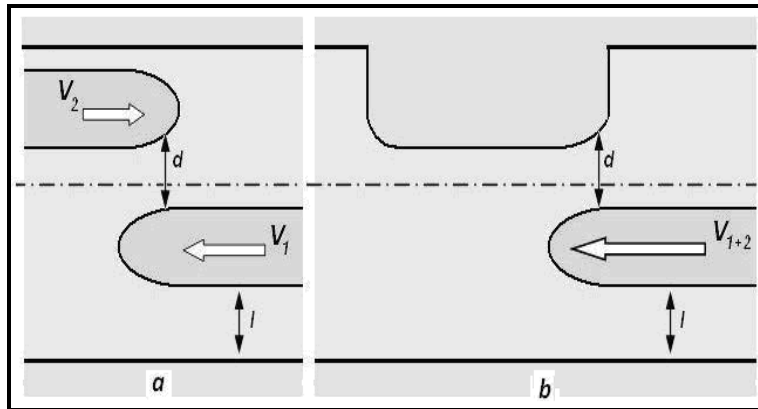repancy of the speeds of both vessels, i.e., $V = V_1 - V_2$. Fig. 5a shows the first stage of overtaking maneuver, when the bow of the vessel «1» passes by the hull of the vessel «2», i.e., $\xi(t) < L_2$. Fig. 5b shows the second stage, which finishes when the stern of the vessel «1» has passed by the bow of the vessel «2», i.e., $\xi(t) < L_1 + L_2$.

Ice impact to the hull of overtaking vessel «1» at a certain point A at the side facing the vessel «2» depends on ice concentration in the area between the vessels hulls d, which varies relative to the initial distance between the vessels centerlines d_0, where ice concentration is considered to be initial. This distance, in its turn, depends on mutual disposition of vessels at the given moment of time, i.e., $\xi(t) = V t$, and on both vessels constructive waterlines coordinates in the considered section a–a relative to centerlines. For the vessel «1», the waterline coordinate can be presented as a function of x, i.e., $y_1(x)$. For the vessel «2» in the expression for waterline coordinate its position should be considered relative to coordinate origin xOy, i.e., $x' = L_2 - \xi + x$. Thus, the distance between vessels in the considered point can be introduces as follows

$$d(\xi, x) = d(t, x) = d_0 - y_1(x) - y_2 \left[L_2 - \xi(t) + x \right] = d_0 - y_1(x) - y_2 (L_2 - Vt + x) \qquad (2)$$

Calculation of ice load to the hull of overtaking vessel «1» is performed starting with the moment of her bow lying abreast the overtaken vessel stern «2» ($t_0 = 0$), and finished when the stern of the vessel «1» lying abreast the bow of the vessel «2» ($t_f = L_2 / V$). For every moment of time: $t_0 \leq t \leq t_f$, ice load calculation is carried out separately for starboard side and port side, by means of integrating along Ox axis from the stem post ($x = 0$) to the abscissa of the stern post of the vessel «2» ($x = \xi$) on the first stage of

overtaking maneuver, and from the abscissa of the stem post of the vessel «2» ($x = \xi - L_2$) to the stern ($x = L_1$) on the second stage of overtaking maneuver. Along the starboard side, ice concentration increasing is considered in the area between the vessels. Along the port side, ice concentration remains initial.

As a base for assessment of ice load to the hull of overtaking vessel, the well-known Eq. [5] is used that gives possibility to calculate ice resistance of the vessel proceeding in broken ice condition.
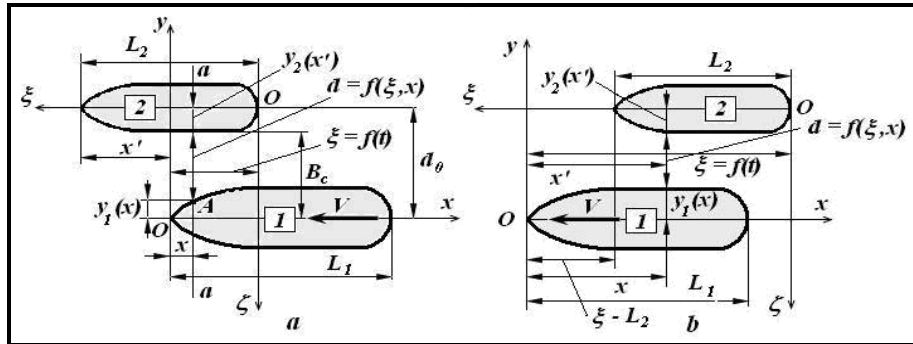
Fig. 5   Schema of overtaking of vessel " «2»" by vessel " «1»": (a)the first stage of overtaking and (b) the second stage.

$$R_s = 10 \left\{ \gamma_{Ice} \sqrt{b_{Ice} \, h_{Ice}} \left(\frac{B}{2} \right)^2 \left[k_1 \left(1 + 2 k_{fr} \, \alpha_b \frac{L}{B} \right) + k_4 \, k_{fr} \, \alpha \frac{L}{B} C_s \right] + \right.$$
$$\left. + k_2 \, \gamma_{Ice} \, b_{Ice} \, h_{Ice} \, B \left(k_{fr} + \beta \cdot tg \alpha_0 \right) \text{Fr} + k_3 \, \gamma_{Ice} \, b_{Ice} \, h_{Ice} \, L \cdot tg^2 \alpha_0 \, \text{Fr}^2 \right\} \qquad (3)$$

In Eq.(3) following notations are applied: R_s: ice resistance for broken ice conditions (without water resistance); b_{Ice}: average: size of ice floes in channel and h_{Ice}: average thickness of ice floes Eq.(1); γ_{Ice}: density of ice; k_{fr}: the ice friction factor against hull plating; C_s: compression of ice cover (balls); L: length and B: width of the vessel; β: waterline area coefficient; α_E: angel between tangent to waterline at nose and center line; k_1, k_2, k_3 empiric coefficients that depend on ice concentration that values were

determined on base of model experiments and real scale vessels trials [5, 8]; Fr is Froude number

$$\mathrm{Fr} = \frac{V}{\sqrt{g\,L}} \qquad (4)$$

Empiric coefficient k_1 depends on ice concentration s (balls) and correlation of vessel beam B and width of the canal B_c, made by ice-breaker, in which the vessel proceeds, that is $B_c/B = m \geq 1$. Formulas to assess the value k_1, obtained by interpolation of experimental data, are the following:

$$k_1(s,m) = 0.01\left[\left(0.25\,s^2 - 2.15\,s + 3.9\right) \times \left(6.9 - m + 0.041\,m^2\right)\right] \quad \text{if } m \leq 12,$$

$$k_1(s,m) = 0.025\left(0.25\,s^2 - 2.15\,s + 3.9\right) \quad \text{if } m > 12, \qquad (5)$$

$$k_1 = 0 \qquad \text{if } s \leq 6.$$

Empiric coefficient k_2 depends only on ice concentration s

$$k_2 = 0.11\,s^2 - 0.2\,s \qquad (6)$$

Coefficients $k_3 = 4.2$, $k_4 = 1.2$, that is constants.

The Eq. (3) for vessel resistance in broken ice includes the three following components:

• Resistance, caused by deformation of ice cover when mowing apart ice floes with the ship's hull in the process of motion and friction of ice floes against the hull (first compound);

• Resistance, connected with friction of ice floes against each other and ice resistance to their motion (second compound);

• Impulse resistance, conditioned by loss of kinetic energy when blowing ice floes against the ship's hull.

Comparison of importance of these components in ice resistance depending on ice concentration shows that if concentration $s > 6$, the value of the first component exceeds the value of the second component more than by an order of magnitude and exceeds the value of the third component by two orders of magnitude. For the described problem, this allows to confine to consideration on the effect of the loads, connected only with mowing apart and friction

of ice floes, to the vessels hull. As a result of this, effect of overtaken vessel on overtaking vessel can be parameterized by means of coefficient k_1 variation, caused by ice concentration variation along the vessel hull and changing of it at every point of waterline in the process of passing by vessels.

Fig. 6 shows the configuration of forces affecting the element of waterline dx at a certain point A: these are the load of moving apart ice floes–N and friction force–S, projection of which to axis of coordinates form on this waterline element dx the ice resistance force dR, side force dF and yawing moment dM.

Using forms for ice loads to the constructive waterline element, cited in Ref. [5] and being the ground for the Eq. (3), the considered values can be represented in the following way:

• Force of ice resistance on the constructive waterline element:

$$dR = k_1(x)\gamma_{Ice}\sqrt{b_{Ice}\,h_{Ice}}\;y_1(x)\left[k_{fr} - y_1'(x)\right]dx \quad (7)$$

• Side force on the constructive waterline element:

$$dF = k_1(x)\gamma_{Ice}\sqrt{b_{Ice}\,h_{Ice}}\;y_1(x)\left[1 - k_{fr}\,y_1'(x)\right]dx \quad (8)$$

• Yawing moment (relative to the vessel bow), appearing on the constructive waterline element:

$$dM = x\,dF - y_1(x)\,dR = k_1(x)\gamma_{Ice}\sqrt{b_{Ice}\,h_{Ice}}\,y_1(x)\,x\left\{1 - \left[y_1'(x)\right]^2\right\}dx \qquad (9)$$
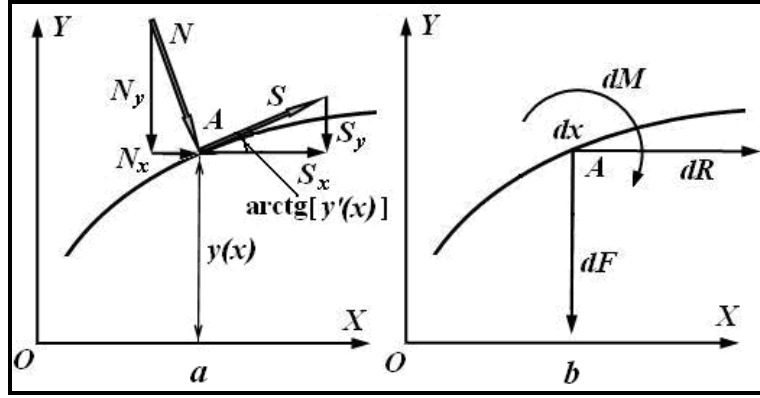
Fig. 6   Configuration of forces affecting the element of waterline dx in point A–(a): N - load of ice floe moving apart, S–ice floe friction force on hull plating, and (b)–resultant action as projections on axes axis: dF–side force, dR–ice resistance and dM–yawing moment.

Changing of ice channel width and, as consequence, ice concentration determines value of the coefficient k_1 during overtaking maneuver. This dependence is parameterized according to the scheme on Fig. 5a, using the Eq. (2) and considering the changing to be inversely proportional to the channel width. Therefore, ice concentration variation can be determined as follows:

$$s(t,x) = s_0 \frac{d_0}{d[\xi(t),x]} = s_0 \frac{d_0}{d_0 - y_1(x) - y_2(L_2 - Vt + x)}. \tag{10}$$

The width of "ice channel" for the adopted model is determined according to the scheme of Fig. 5 in the following way

$$B_c(\xi,x) = \\ = 2[d_0 - y_2(x)] \tag{11}$$

Consequently, relative width of "ice channel" as the function of time is the following

$$m(t,x) = \frac{2}{B}[d_0 - y_2(L_2 - Vt + x)] \tag{12}$$

The opposite port side of overtaking vessel is affected also by ice loads, value of which, applied to the waterline element, are determined by the Eq. (7)–(9). In these formulas, the value of coefficient k_{10} corresponds to initial ice compaction s_0 and relative width of ice canal $m > 12$. Thus,

$$k_1(t,x) = 0.01\left[\left(0.25 s^2(t,x) - 2.15 s(t,x) + 3.9\right) \times \left(6.9 - m(t,x) + 0.041 m^2(t,x)\right)\right] \tag{13}$$

$$k_{10} = 0.025\left(0.25 s_0^2 - 2.15 s_o + 3.9\right)$$

In the considered problem, the ice loads appearing in the process of passing by vessels are of great interest. These values can be defined as difference of loads to port side and starboard side in the considered section at a distance of x from the stem of overtaking vessel «l» in the form of the following expressions

- Additional ice resistance:

$$dR_s(t,x) = \left[k_1(t,x) - k_{10}\right]\gamma_{Ice}\sqrt{b_{Ice}\,h_{Ice}}\, y_1(x)\left[k_{fr} - y_1'(x)\right]dx \tag{14}$$

- Side force:

$$dF_s(t,x) = \left[k_1(x) - k_{10}\right]\gamma_{Ice}\sqrt{b_{Ice}\,h_{Ice}}\, y_1(x)\left[1 - k_{fr}\, y_1'(x)\right]dx \tag{15}$$

- Yawing moment:

$$dM_s(t,x) = \left[k_1(t,x) - k_{10}\right]\gamma_{Ice}\sqrt{b_{Ice}\,h_{Ice}}\, y_1(x)\, x\left\{1 - \left[y_1'(x)\right]^2\right\}dx \tag{16}$$

Total ice loads for every moment of time t are determined by integrating these expressions along the axis x (Fig. 5). Integration limits are different for every stage of overtaking, as shown in Fig. 5. For the first stage of overtaking, integration is performed within the limits from the overtaking vessel bow ($x = 0$) to the coordinate of overtaken vessel stern ($x = \xi(t)$), that is for $\xi(t) \le L_2$, following formula was applied:

$$R_s(t) = \gamma_{Ice}\sqrt{b_{Ice}\,h_{Ice}}\int_0^{\xi(t)}\left[k_1(t,x) - k_{10}\right]y_1(x)\left[k_{fr} - y_1'(x)\right]dx \tag{17}$$

$$F_s(t) = \gamma_{Ice}\sqrt{b_{Ice}\,h_{Ice}}\int_0^{\xi(t)}\left[k_1(x) - k_{10}\right]y_1(x)\left[1 - k_{fr}\,y_1'(x)\right]dx \tag{18}$$

$$M(t) = \gamma_{Ice}\sqrt{b_{Ice}\,h_{Ice}}\int_0^{\xi(t)}\left[k_1(t,x) - k_{10}\right]y_1(x)x\left\{1 - \left[y_1'(x)\right]^2\right\}dx \tag{19}$$

For the second stage of overtaking, integration is performed from the coordinate of overtaken vessel bow «2» ($x = L_2 - \xi(t)$) to the overtaken vessel stern «1» ($x = L_1$), so for $\xi(t) > L_2$ the appropriate formulas are the following:

$$R_s(t) = \gamma_{Ice}\sqrt{b_{Ice}\,h_{Ice}}\int_{\xi(t)-L_2}^{L_1}\left[k_1(t,x) - k_{10}\right]y_1(x)\left[k_{fr} - y_1'(x)\right]dx \tag{20}$$

$$F_s(t) = \gamma_{Ice}\sqrt{b_{Ice}\,h_{Ice}}\int_{\xi(t)-L_2}^{L_1}\left[k_1(x) - k_{10}\right]y_1(x)\left[1 - k_{fr}\,y_1'(x)\right]dx \tag{21}$$

$$M_s(t) = \gamma_{Ice}\sqrt{b_{Ice}\,h_{Ice}}\int_{\xi(t)-L_2}^{L_1}\left[k_1(t,x) - k_{10}\right]y_1(x)x\left\{1 - \left[y_1'(x)\right]^2\right\}dx \tag{22}$$

Thus, analytic model of vessels interaction when passing by in the ice channel includes:

• Expressions for additional ice resistance to motion, side force and yawing moment Eq. (17)–(22);

• Expressions for empiric coefficients k_1 and k_{10}, parameterizing ice impact to vessel hull (13);

• Expression for concentration variation while overtaking (10);

• Expression for variation of relative ice canal width (area between vessels) while overtaking Eq. (12).

The same model can be used without any changes for on-coming passing by vessels. For this purpose in the Eq. (10) and (12) as a speed V the summary of the vessels speeds «1» and «2» should be used, that is $V = V_1 + V_2$, and expression for the constructive waterline $y_2(x)$ should be changed (represented relative to midship).

To solve the task of ice loads to overtaken vessel, the given model can be used as well. For this purpose, origin of coordinates Oxy should be connected with the stern of overtaken vessel, while origin of coordinates $O\xi\zeta$ should be connected with the bow of overtaking vessel.

4. The Method for Calculation of Loads, Appearing When Vessels Passing by in Ice Channel

To use the above described model, it is necessary to represent constructive waterlines of interacting vessels $y1(x)$ and $y2(x')$ in analytic form. Considering the main effect of interaction is connected with ice loads, waterline form approximation can be significantly facilitated. For this purpose, the following analytic presentation, accounting for occurrence of dead flat in the hull with the length of L_{f1}, situated symmetrically relative to midship frame was applied:

$$y_1(x) = 0.5B_1 \left\{ 1 - \left[1 - \frac{x}{0.5(L_1 - L_{f1})} \right]^{\frac{L_1 - L_{f1}}{B_1} \operatorname{tg} \alpha_{0/1}} \right\} \quad \text{if } 0 \leq x \leq 0.5(L_1 - L_{f1}),$$

$$y_1(x) = 0.5B_1 \quad \text{if } 0.5(L_1 - L_{f1}) \leq x \leq 0.5(L_1 + L_{f1}), \tag{23}$$

$$y_1(x) = 0.5B_1 \left\{ 1 - \left[1 + \frac{x - L_1}{0.5(L_1 - L_{f_1})} \right]^{\frac{L_1 - L_{f1}}{B_1} \operatorname{tg} \alpha_{20/1}} \right\} \quad \text{if } 0.5(L_1 + L_{f1}) \leq x \leq L_1.$$

In these formulas, α_{20} is the angle of the waterline inclination to the centerline in the aft part.

Differentiation of these expressions allows finding equation for derivate $y'(x)$ or angle of waterline inclination relative to the centerline α_w.

$$\alpha_{w1}(x) = -\operatorname{arctg} \left\{ (\operatorname{tg} \alpha_{0/1}) \left[1 - \frac{x}{0.5(L_1 - L_{f1})} \right]^{\frac{L_1 - L_{f1}}{B_1 \operatorname{ctg} \alpha_{0/1}} - 1} \right\} \quad \text{if } 0 \leq x \leq 0.5(L_1 - L_{f1}),$$

$$\alpha_{w1}(x) = 0 \quad \text{if } 0.5(L_1 - L_{f1}) \leq x \leq 0.5(L_1 + L_{f1}), \tag{24}$$

$$\alpha_{w1}(x) = -\operatorname{arctg} \left\{ (\operatorname{tg} \alpha_{20/1}) \left[1 + \frac{x - L_1}{0.5(L_1 - L_{f1})} \right]^{\frac{L_1 - L_{f1}}{B_1 \operatorname{ctg} \alpha_{20/1}} - 1} \right\} \quad \text{if } 0.5(L_1 + L_{f1}) \leq x \leq L_1.$$

Fig. 7 shows the form of the waterline and variation of angles of its inclination to the centerline, determined by the Eq. (23) and (24).

Similar (23) for the form of constructive waterline is applied to overtaken vessel. For this purpose, it is necessary to produce appropriate changing vessel size

$$y_2(x) = 0.5B_2 \left\{ 1 - \left[1 - \frac{L_2 - Vt + x}{0.5(L_2 - L_{f2})} \right]^{\frac{L_2 - L_{f2}}{B_2} \operatorname{tg} \alpha_{0/2}} \right\} \quad \text{if } L_2 - Vt + x \leq x \leq 0.5(L_2 - L_{f2}),$$

$$y_2(x) = 0.5B_2 \quad \text{if } 0.5(L_2 - L_{f2}) \leq L_2 - Vt + x \leq 0.5(L_2 + L_{f2}), \tag{25}$$

$$y_2(x) = 0.5B_2 \left\{ 1 - \left[1 + \frac{L_2 - L_1 - Vt + x}{0.5(L_2 - L_{f_2})} \right]^{\frac{L_2 - L_{f2}}{B_2} \operatorname{tg} \alpha_{20/2}} \right\} \quad \text{if } 0.5(L_2 + L_{f2}) \leq L_2 - Vt + x \leq L_2.$$
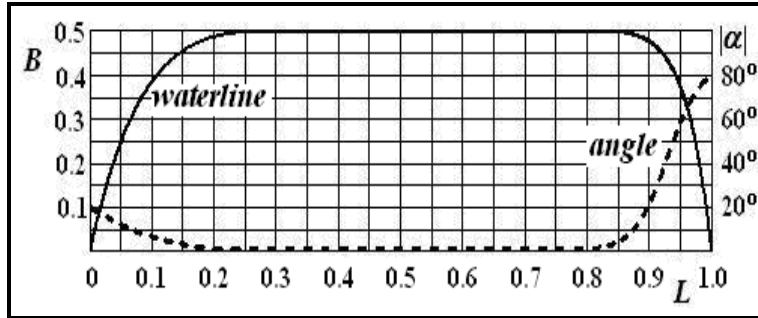
Fig. 7 Form of waterline and angles of its inclination relative to vessel midline in accordance with Eq. (23) and (24).

and origin of coordinate of considered section also. After forms conversion following forms was obtained was obtained Eq. (23) and (25) were applied for derivation of dependency of ice concentration $s(t_i, x)$ and relative width of ice canal $m(t_i, x)$ on x coordinate for every moment of time within the range $0 \leq t_i \leq t_f = (L_1+L_2)/V$. This allowed to determine the kind of dependency of coefficient $k_1(s, m)$ on coordinate x for the same moments of time, i.e., $k_1(t_i, x)$. The obtained expression combined with Eq. (17)–(19) and Eq. (20)–(22) was used to calculate ice loads, namely, additional ice resistance, side force and yawing moment by means of integration along the x axis using the Eq. (23)–(25) according to the stage of overtaking.

The calculations were performed using MathCAD systems. As the initial data the vessels sizes, their speeds, distance between vessels motion trajectories were given. Ice conditions were characterized by ice thickness and concentration in the navigable ice channel. To research influence of vessels size, their speeds and ice conditions to the ice loads, the above mentioned parameters were varied within the ranges of interest.

5. Results Assessment of Calculation of Ice Loads to the Vessel Performing Overtaking Maneuver in Ice Channel

The main option to research vessels interaction in the course of overtaking maneuver is considering the following initial data:

- The overtaking vessel «1» had length $L_1 = 120$ m and width $B_1 = 20$ m;
- The overtaken vessel «2» had length $L_2 = 90$ m and width $B_2 = 16$ m;
- Speed of the overtaking vessel «1» exceeded one of the overtaken vessel «2» by $V = 3$ m/sec,
- Ice thickness $h = 0.5$ m and concentration $s = 7$ balls.

Values of additional ice resistance and side force affecting the overtaking vessel «1» were normalized by the value $0.5 \cdot \rho \cdot V^2 \cdot L_1 \cdot B_1$, and value of yawing moment by value $0.5 \cdot \rho \cdot V^2 \cdot L_1 \cdot B_1^2$. Therefore, coefficients of additional ice resistance C_R, side force C_F and yawing moment C_M are analyzed further.

Fig. 8 shows changing of coefficients of additional ice resistance C_R, side force C_F and yawing moment C_M in the process of overtaking. In order to represent all ice loads in one diagram, the yawing moment coefficient is reduced by 5 times. Following moments of time are marked:

T_{b1-s2} - when the bow of the vessel «1» is abeam the stern of the vessel «2» (beginning of overtaking);

T_{b1-b2} - the bow is abeam the bow of the vessel «2»;

T_{s1-s2} - beam of stern parts of the vessels;

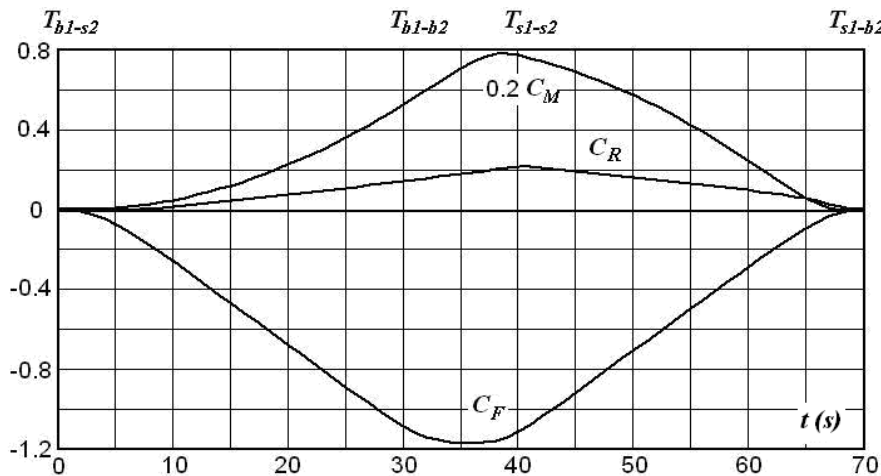T_{s1-b2} - completing of overtaking (beam of the stern of the vessel «1» and the bow of the vessel «2»).

Fig. 8   Variation of coefficients: additional ice resistance C_R, side force C_F and yawing moment C_M, affecting overtaking vessel during passing.

Difference form (asymmetrical effect) of curves of ice loads coefficients depending on time in initial and completive stages of overtaking should be taken into consideration. This effect can be explained by asymmetrical of hull forms of bow and stern of vessels (Fig. 7).

Dependencies of ice loads to overtaking vessels on time or on position relative to overtaken vessel have expressed slightly asynchronous maximums:

• Maximum of additional ice resistance at $t \cong 40.1$ sec after start of the overtaking maneuver;

• Maximum of side force at $t \cong 35.7$ sec;

• Maximum of the yawing moment $t \cong 38.5$ sec.

Further, when assessing impact of ice conditions and other factors to ice loads, only maximum values of loads are considered. Side force arising at the overtaking vessel is negative (directed opposite to an axis Oy. Then its absolute value is described.

Direction and behavior of side force and yawing moment in the course of overtaking in the ice channel differ of those arising in water area free of ice. Particularly, side force has opposite direction (not to overtaken vessel, but to the edge of the canal). Yawing moment determined relative to the bow of the overtaking vessel has direction that corresponds to the turn of the bow to the overtaken vessel, whilst the stern–to the ice channel edge, and is not changed direction in the course of overtaking. Fig. 9 illustrates the tendency of yawing of ships in the course of overtaking and the dangers of mutual collision and blow by a stern about an edge of the ice channel caused by it.

This conclusion conforms to the results of modeling tests performed before in the ice-towing tank [6, 7]. Behavior of additional ice resistance, side force and yawing moment in the course of overtaking maneuver also corresponds to modeling experimental results. Direct comparison of calculation results with modeling data cannot be correct, since the measured values of loads contain random fluctuations caused by cracking and fracture of separate ice floes in the area

between vessels, which are commensurable to abeam distance between vessels.

Overtaking speed variation, i.e., difference of speeds of interacting vessels does not result in changing coefficients values of ice loads C_R, C_F and C_M, affecting the overtaken vessel.

Special research was also performed concerning impact of minimum abeam distance between vessels sides and ice concentration on maximum values of ice forces and moment, affecting the overtaking vessel. Results of calculations are presented in Figs. 10-12.

The value of maximum abeam distance d_T is rated to the beam of the overtaking vessel. These data show that when decreasing abeam distance between vessels sides, ice loads to the overtaking vessel increase. In correlation of ice loads coefficients with ice concentration, there is maximum in the concentration range 6 balls $< s <$ 8 balls. Presence of ice loads maximum can be explained in the following way. In case of little ice compaction within the range: $0 < s < 6$, ice loads growth along with increasing of ice concentration is connected with raising of difference between ice concentration in the area between vessels boards and ice concentration at the opposite side. If concentration is considerable $s > 8$, this difference reduces, as ice concentration between vessels boards cannot exceed value $s = 10$ balls. Allocation of ice loads maximum displaces towards the greater concentrations under decreasing distance between vessels boards.
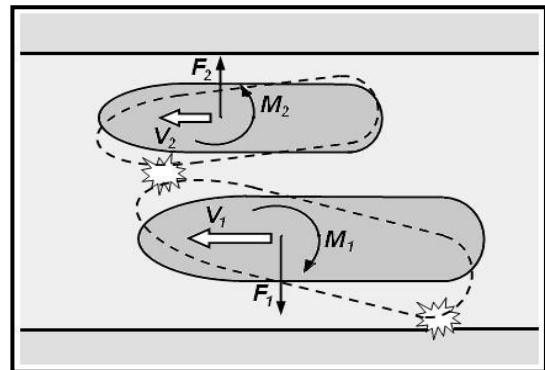
Fig. 9 Tendency to yawing of vessels during overtaking and dangerous of mutual collision or blow to ice channel edge caused by this passing.
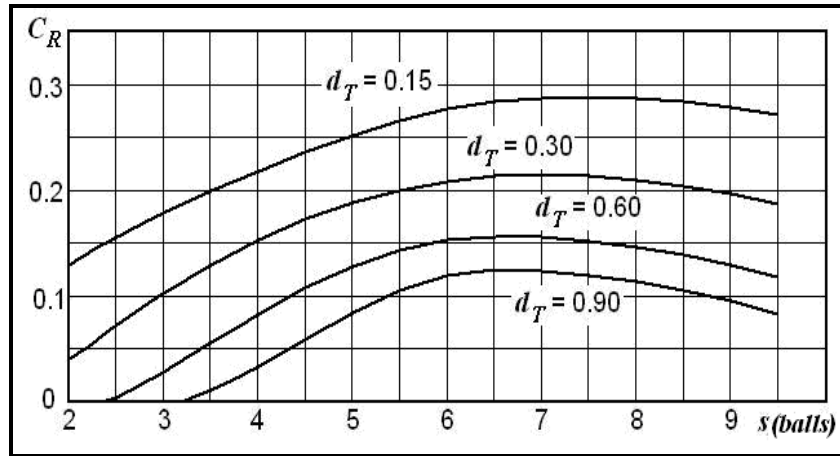
Fig. 10   Dependence of the additional ice resistance coefficient C_R on minimal abeam distance between boards of vessels d_T and ice concentration s.
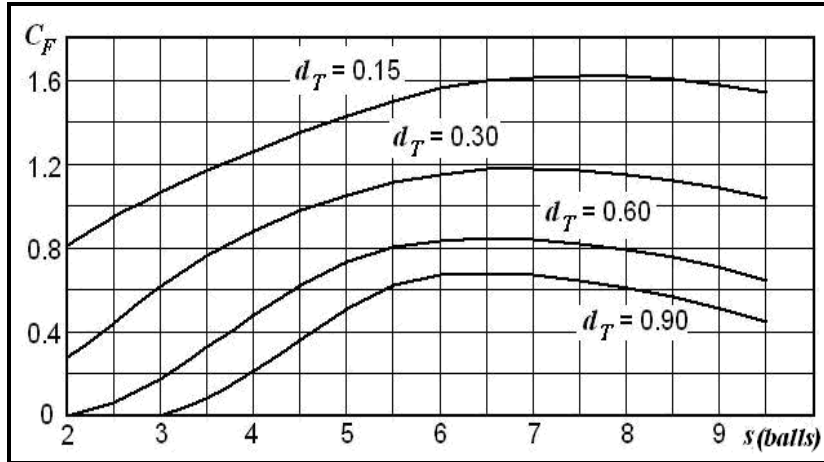
Fig. 11   Dependence of the side force coefficient C_F on minimal abeam distance between boards of vessels d_T and ice concentration s.
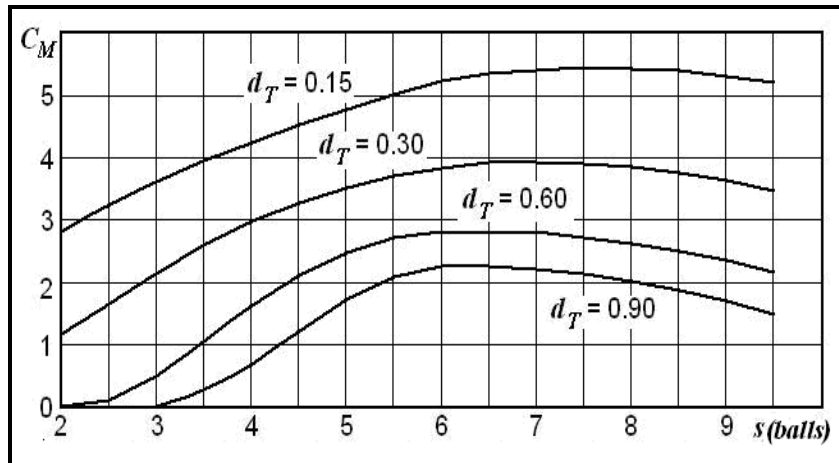
Fig. 12   Dependence of the yawing moment coefficient C_M on minimal abeam distance between boards of vessels d_T and ice concentration s.
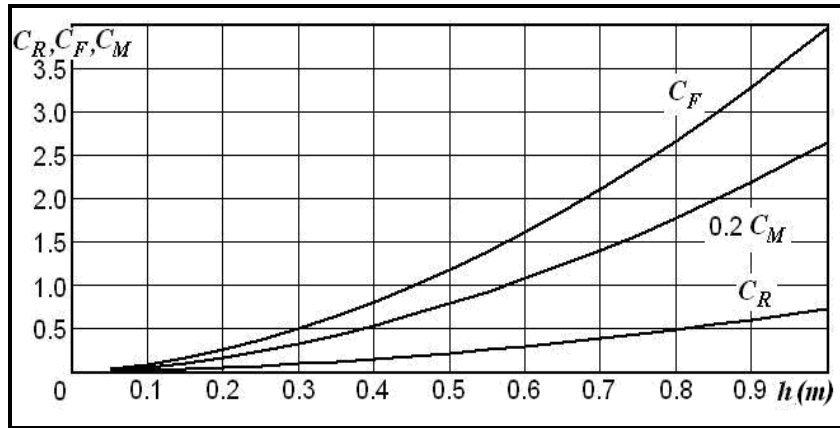
Fig. 13 Variation of the ice loads coefficients affecting overtaking vessel in dependence on the thickness of ice floes within navigable ice channel.
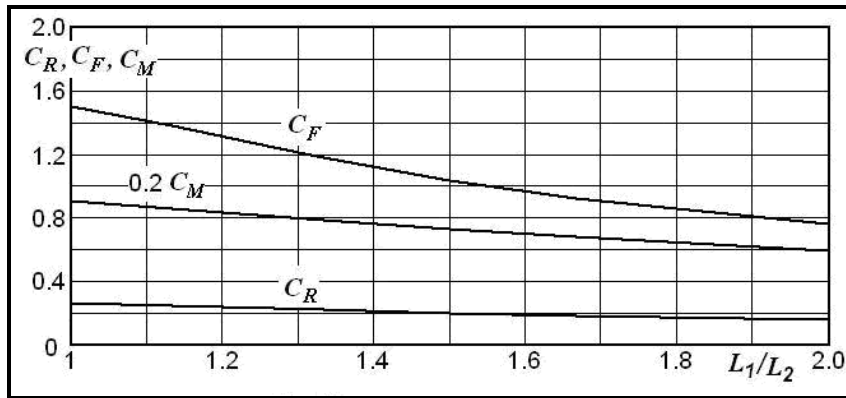
Fig. 14 Variation of the ice loads coefficients affecting overtaking vessel under increase its hull length in relation to length of overtaken vessel (L_1/L_2).

Fig. 13 shows changing maximum values of ice loads to the overtaking vessel when increasing thickness of ice floes filling the ice canal at concentration $s = 7$ balls and relative abeam distance between vessels $d_T = 0.30$. Ice loads increase connected with ice thickness raise is natural, and the presented results demonstrate mainly intensity of this growth. For example, when in case of twofold increase of ice thickness: from $h = 0.4$ m to $h = 0.8$ m, ice loads coefficients grow approximately by 3.34.

Fig. 14 shows the research results of impact of interacting vessels dimensions ratio (ratio of hulls lengths L_1/L_2) on maximum values of ice loads on the overtaking vessel. When modeling, relative minimum abeam distance between vessels d_T remained constant, ice thickness $h = 0.5$ m and compaction $s = 7$ balls. These data show that with increasing relative

dimensions of overtaking vessel, ice loads caused by interaction with the overtaken vessel decrease considerably. When increasing dimensions of the overtaking vessel to double in comparison with the overtaken vessel, side force decreases approximately by half, and additional ice resistance and yawing moment diminish by 1.5.

6. Conclusions

As a result of the carried out research, the mathematical model of vessels interaction when proceeding in navigable ice channel filled with broken ice was created. The model is based on parameterizing of ice loads to the hull by two principal forces: normal, connected with moving ice floes apart, and tangent, connected with friction of ice floes with the hull plating. As a result of computer-based modeling with

the use of the model, ice loads values to the interacting vessels can be determined, namely additional ice resistance, side force as well as yawing moment depending on the dimensions of the vessel, their speeds, and ice channel size and features of broken ice in the canal.

To demonstrate capabilities of the developed model, the modeling of ice loads to the overtaking vessel was performed, dependence of these loads on compaction and thickness of broken ice in the ice canal, on abeam distance between vessels and on correlation of the vessels dimensions was examined. The obtained results correspond to the model experiments performed earlier in the ice towing tank in a quality manner.

Considerable result is the confirmation by theoretical analysis of qualitative difference of vessel interaction when passing in ice condition and in water area free of ice, established earlier in model experiment. Advancing of the theoretical solution and mathematical model allowed specifying results of the research carried out earlier, presented in the publications [5, 6] and concerning the behavior of side force and yawing moment in the process of passing by vessels.

The developed model of vessels interaction is recommended to use in navigational simulators for the purpose of training deck officers to handle a vessel when proceeding in the navigation ice channel.

Hereafter, it is intended to perform further improvement of the theoretical model that will allow considering disposition of vessels relative to borders of the ice channel when calculating ice loads. This will enable to develop recommendations on the choice of cross sectional dimension of navigable ice channel, providing safety of navigation as well as to advise safe conditions of vessels traffic in the channel relative to speed of vessels and the distance between on-coming and overtaken vessels and also between vessels and borders of the canal.

It is intended to carry out analytical modeling of the experiments performed earlier in the ice towing tank as well. The obtained results will be compared to the experimental data which will be processed specifically: filtering of random fluctuations within results of measurements of ice loads to the models of interacting vessels.

Acknowledgement

References

[1] I. Arikainen, K.N. Chubakov, Alphabet of Ice Navigation, Transport, Moscow, 1987, p. 224.

[2] J. Falter, Validation of a potential flow code for computation of ship-ship interaction forces with captive model test results, M.Sc. Dissertation, Ghent University, Belgium, 2010.

[3] J. King, Unsteady Hydrodynamic interactions between ships in shallow waters, in: Proceedings of 6th Australasian Hydraulic and Fluid Mechanics Conference, Adelaide, Australia, 1977.

[4] B.P. Ionov, E.M. Gramuzov, Ice Propulsion of Vessels, Sudostroenie, Leningrad, 2001, p. 486.

[5] V.I. Kashtelian, I.I. Pozniak, A.Ia. Ryvlin, Ice Resistance for Ship Motion, Sudostroenie, Leningrad, 1968, p. 238.

[6] V.K. Goncharov, N.Yu. Klementieva, K.E. Sazonov, Interaction of vessels at traffic in the ice channel, in: Proceedings of the 16th International Conference of Ship and Shipping Research (NAV 2009), Messina, Italy, Vol. 2, 2009.

[7] V.K. Goncharov, N.Yu. Klementieva, K.E. Sazonov, Interaction of ships under navigation in ice conditions, in: Proceedings of NAV 2012, 17th International Conference on Ships and Shipping Research [CD-ROM]. Naples, Italia, Extended Abstract, Full text, 2012.

[8] A.I. Ryvlin, D.E. Kheisin, Field Tests of Ships in Ice Conditions, Sudostroenie. Leningrad, 1980 p. 208.

[9] V.K. Goncharov, N.Yu. Klementieva, K.E. Sazonov, Ice makes difference, The Naval Architect Febr. (2009) 16-19.

[10] V.K. Goncharov, N.Yu. Klementieva, K.E. Sazonov, Interaction of ships under traffic within navigable ice channel, in: The Proceedings of the 22nd International Conference on Port and Ocean Engineering under Arctic Conditions (POAC'13), Espoo, Finland, USB Memory Stick, Paper No. 58, 2013.

A Hybrid Particle-Grid Scheme for Computing Hydroelastic Behaviors Caused by Slamming

Hidemi Mutsuda[1], Suandar Baso[2] and Yasuaki Doi[1]

1. Division of Energy and Environmental Engineering, Hiroshima University, Higashi-Hiroshima city *739-8527, Japan*

2. Department of Naval Architecture, Faculty of Engineering, Hasanuddin University, South Sulawesi *90245, Indonesia*

Abstract: Capable and accurate predictions of some effects of strongly nonlinear interaction wave-ship associated with hydroelastic behaviors are very required for simulation tool in naval architect and ocean engineering. It can guarantee ship safety at the sea state by producing proper design. Therefore, we have developed a hybrid scheme based on both grid and particle method. In order to clarify hydroelastic behaviors of a ship, a dropping test of a ship with elastic motion has been performed firstly. The developed scheme has been then validated on ship dropping case under the same conditions with experiment. The comparisons showed consistently in good agreement. Furthermore, evaluation on hydroelastic behaviors of ship motion under slamming, the impact pressure tends to increase in increasing Froude number. (F_n) The bending moment and torque defined at the centre gravity due to hogging and sagging events can be predicted well, and their effects on the ship increase in increasing wave length even though the impact pressure decreases in increasing wave length after wave length λ/L, where L is ship length, is equal to 1.0. Moreover, hydroelastic behaviors affect the large heave and pitch amplitudes. Finally, the developed scheme can predict simultaneously hydrodynamic and hydroelastic with a strongly nonlinear interaction between wave and ship.

Key words: Impact pressure, ship slamming, hydroelasticity, grid based method, particle based method.

1. Introduction

In sea state, a ship moving forward in severe wave condition can cause wave impact loads on its surface during short time such as slamming event and it is vulnerable to some effects caused by that slamming impact. In addition, the wave load acting on a ship under strongly interaction wave-ship can generate an impact pressure and also accelerate a fatigue failure at the same time which influences on ship performance, ship structure and passenger comfort.

Moreover, a ship is not a really rigid construction and this means that a ship has elastic behaviors where it experiences strains and stresses because of its structural flexibility. This cannot be neglected that hydroelastic behaviors of a ship contributes some effects to ship performances. Hence, hydroelastic behaviors of a ship have to be considered in predicting

ship motions, pressure, bending moment and torque as resulted by the strongly interaction between wave-ship associated with hydroelastic effects toward proper ship design and ship safety.

The concept that a ship can be modelled as elastic beams structures was firstly given by Inglis [1] and later coined firstly the term hydroelasticity by Heller and Abramson [2] that the fluid pressure acting on the structure modifies its dynamic state and, in return, the motion and distortion of the structure disturb the pressure field around it. Then, the study of the 2D (two-dimensional) hydroelasticity theory of ships was established by Bishop and Price [3].

By beginning the research results of von Karman [4] and Wagner [5], the research of water impact with free surface flows have been investigated numerically and experimentally, e.g., identification experimentally of the impact of surface planes and the entrained air effect [6], time dependent water entry for wedges of various angles [7, 8], and a comparison of the

---

Corresponding author: Hidemi Mutsuda, Ph.D., research field: environmental fluid engineering. E-mail: mutsuda@hiroshima-u.ac.jp.

maximum impact pressure of a symmetrical wedge [9]. The slamming loads of 2D symmetrical section were investigated by using Boundary Element Method and also the effect of flow separation for axisymetric impact [10-12]. However, some investigations cannot adequately handle flow with water impact involving plugging waves and air bubbles.

Over the past 40 years, Faltinsen [13, 14] gave a clear definition of the term ship hydroelasticity that the water pressure acts on the structure and the structure deforms. At the same time, the speed of the structural deformation influences the pressure in the water. The hydroelastic formulation and model slamming was investigated by Bereznitski et al., [15-18] using numerical model, Tajima and Yabe [19] simulated a vessel slamming by using CIP (Constrained Interpolation Profile Scheme) Then, wave loads on a ship in waves using an elastic model was studied and verified with full scale measurement [20]. Moreover, Faltinsen [21, 22] presented water entry of a wedge by hydroelastic orthotropic plate theory and an approximate 3D (three-dimensional) theoretical investigation of hydroelastic wetdeck slamming, and also presented a theoretical study of representing the wetdeck as a beam model and accounting for dynamic hydroelastic effects. Senjanovic et al. [23] analyzed the hydroelastic effect on a flexible segmented barge motion in waves and distortion and slam events was characterized experimentally by using a hydroelastic segmented model [24].

Recently, many ongoing research in marine engineering have been attempted to yield CFD (Computational Fluid Dynamics) tool toward accurate tool with considering CFD requirements. These can predict wave impact as hydrodynamic effects due to strongly nonlinear wave-body interactions; however, involvement of hydroelastic effects associated with capturing nonlinear free surface flows on a ship motion under severe wave condition is still rarely devoted and the results have

been generally concerned on water entry problems with capturing technique of free surface phenomena or with a weakly interaction between wave and an elastic ship. The nonlinear free surface flows are difficult because it is a complex problem to keep the sharpness of the air-water interface tolerable and to handle moving free surface and elastic ship boundary. In addition, the solutions of CFD for ship motion simulation require more quantitative assessments in reproducibility and validation. Therefore, the developments of CFD techniques to predict accurately hydrodynamic and hydroelastic effects on ship motion in severe wave condition need tremendous efforts.

In our previous works, our developed method was applied to seakeeping performace in nonlinear waves with breaking [25, 26]. In present study, our developed method, a hybrid particle-grid scheme, has been verified its usefulness in predicting hydroelastic effects on a ship motion in nonlinear wave with breaking. Here, the ship has been considered as an elastic body in both numerical simulation and experimental work. In addition, some phenomena of nonlinear free surface flow caused by strongly interaction between wave-elastic ships have been captured as well. The hybrid particle-grid scheme is a coupled Eulerian grid and Lagrangian particles which combines CIP method [27] and SPH method [28] to combine advantages and to compensate disadvantages of the both particle-grid methods. The advantages and disadvantages of the both methods are stated clearly in our previous publication [26]. The model has two kinds of Lagrangian particles, i.e., SPH and free surface particle, on Eulerian grids to correct interface tracking error. The two types of Lagrange particles are collocated and attracted with highly accurate captured nonlinear free surface under resolved region with Eulerian grid.

In this study, the experimental work of ship dropping test has been performed and it has been simulated numerically as well under the same

conditions. Furthermore, the developed method, a hybrid particle-grid scheme, has been applied to elastic ship motion in nonlinear wave with breaking to predict and clarify impact pressure, bending moment, heave and pitch motions, and some phenomena caused by nonlinear interaction ship-wave with hydroelastic behaviors.

2. Computational Method

In this section, the numerical method, which combines the Eulerian scheme and the Lagrangian particles by coupling the SPH method and CIP method with particle, are described concisely. More detail explanations were stated in the previous publications [25, 26]. First, the CIP method with particles is introduced as a numerical scheme that combines the accuracy of Lagragian front tracking. Thereafter, the SPH method is employed to calculate deformation, strain, stress of elastic body, and 3D motion.

2.1 Arrangement of Grids and Particles

The developed Eulerian scheme with Lagrangian particles has been illustrated as shown in Fig. 1. This scheme uses a staggered grid system and has two types of Lagrange particles, i.e., SPH particles to describe solid and free surface particles to capture free surface accurately.

Density function ϕ_I defined on a grid node is corrected by using density function ϕ_P on free surface particles within referenced area with radius h. A smooth approximation of a density function can be constructed by using a Kernel function in the SPH method.

2.2 Governing Equations for Fluid Phase

The governing equations for fluid phase consist of the mass conservation equation, incompressible Navier-Stokes equation and the equation of continuity, I-phase density function φ_I $(0 \leq \varphi_I \leq 1)$ and its advection equation. The equations are expressed as follows:
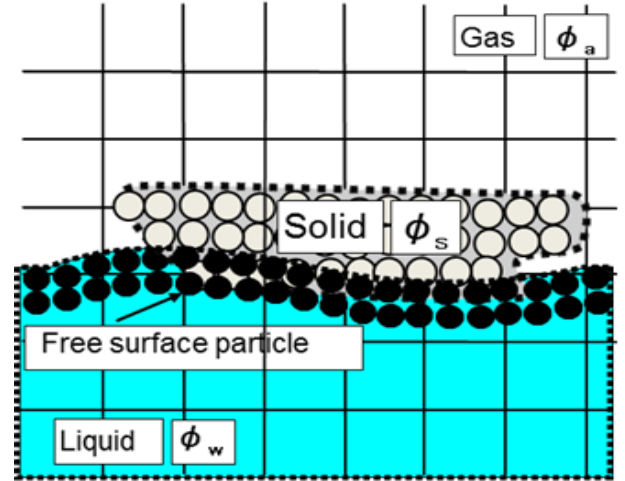
Fig. 1 Illustration of the proposed model (indicates density function; Lagrangian particles are located on Eulerian grid)

$$\frac{\partial \overline{u}_i}{\partial x_i} = 0 \tag{1}$$

$$\frac{\partial \overline{u}_i}{\partial t} + \overline{u}_j \frac{\partial \overline{u}_i}{\partial x_j} = -\frac{1}{\rho}\frac{\partial \overline{P}}{\partial x_i} - \frac{\partial \tau_{ij}}{\partial x_j} + \frac{\mu}{\rho}\frac{\partial^2 \overline{u}_i}{\partial x_j \partial x_j} + g_i + \overline{F}_{fsi} \tag{2}$$

$$\frac{\partial \varphi_I}{\partial t} + \overline{u}_j \frac{\partial \varphi_I}{\partial x_j} = 0 \tag{3}$$

where, u_i is the velocity, μ is the coefficient of fluid viscosity, ρ is the fluid density, P is the pressure, F_{fsi} is the fluid-structure interaction, g_i is the acceleration due to garvity, τ_{ij} is the SGS stress term, and ϕ_I is the density function. To reduce model parameters, the SGS stress term is solved by using the Dynamic SGS Model. More details are provided by Mutsuda and Yasuda [29].

2.3 Advection Step and Non-Advection Step

The governing equations are solved by using the splitting method which is suitable for solving a multi-phase flow without smearing a density across interface between air and water. The advection step is calculated by the CIP method proposed by Takewaki and Yabe [30]. Then, the Type-M scheme of the CIP method is employed by using the third-order accuracy in time and space [27]. On the other hand, the non-advection step is solved by using the second-order finite difference method.

2.4 Governing Equations for Solid Phase

The governing equations for solid phase are the continuity and momentum equations as follows:

$$\frac{D\rho}{Dt} + \rho\frac{\partial u^i}{\partial x^i} = 0 \tag{4}$$

$$\rho\frac{Du^i}{Dt} = \frac{\partial \sigma^{ij}}{\partial x^j} + g^i - F_{fsi}^i \tag{5}$$

where, ρ is the density, u_i is the velocity, $P = -\sigma_{kk}/3$ is the pressure, x^j is the position vector of vector j components, σ_s^{ij} is the stress tensor of the solid phase, and F_{fsi} is the fluid structure interaction term. The stress tensor σ_s^{ij} in Eq. (5) is given by

$$\sigma_s^{ij} = -P\delta^{ij} + S^{ij} \tag{6}$$

where, S^{ij} is the deviatoric stress tensor, the pressure solved by the Poisson's Eq. (9) as mentioned below.

The preset numerical model considers a large deformation of an elastoplastic body. The solid body changes at every calculation step by using the following equation:

$$\{dS^{ij}\} = [D^{ep}]\{d\varepsilon^{ij}\} \tag{7}$$

where, D^{ep} is the elastoplastic matrix, $d\varepsilon^{ij}$ the time increment of the strain, and dS^{ij} the time increment of the deviatoric stress. To solve rotation of the solid phase during a deformation, the Jaumann derivative is used to ensure material frame indifference with respect to the rotation as follow:

$$\frac{dS^{ij}}{dt} = 2\mu\left(\dot{\varepsilon}^{ij} - \frac{1}{3}\delta_{ij}\dot{\varepsilon}^{ij}\right) + S^{ik}\Omega^{jk} + \Omega^{ik}S^{kj} \tag{8}$$

where, $\dot{\varepsilon}$ is the strain rate tensor and Ω the spin tensor. Other details are given by Mutsuda et al. [31].

The pressure with specified jump conditions is solved by the Poisson's equation given by

$$\nabla \cdot \left(\frac{\nabla P^{n+1}}{\rho^*}\right) = \frac{\nabla \cdot u^*}{\Delta t} \tag{9}$$

Where, $*$ denotes a physical value after the advection step. The pressure for solid phase can be obtained by

this equation and be applied in solving a solid deformation.

The fluid structure interaction F_{fsi} is solved by acceleration obtained from the pressure on the SPH particles interpolated using the pressure on grids solved by the Poisson's Eq. (9). In the model, the fluid structure interaction F_{fsi} in Eqs. (2) and (5) can be given by the following equation:

$$F_{fsi}(\mathbf{r}_a) = -\frac{1}{\rho(\mathbf{r}_a)}\sum_b m_b \frac{P(\mathbf{r}_b)}{\rho(\mathbf{r}_b)}\nabla_a W(\mathbf{r}_a - \mathbf{r}_b, h) \tag{10}$$

where, r is location vector of particles in 3D, P is pressure on a particle, ρ is density, m is mass, h is reference area and W is Kernel function. To keep computational efficiency and stability, the time increment in the solid phase is approximately 1/10 to 1/50 of that in fluid phase.

2.5 Ship Motions

A ship motion is solved by using information obtained from SPH particles because a ship hull consists of SPH particles capturing motion and deformation of a ship. Therefore, the 3D motion of a ship hull is represented by describing translation and rotation of the center of gravity of a ship hull by using the following equations:

$$\frac{\partial^2 x_{s,k}}{\partial t^2} = \frac{F_{s,k}}{m_i} - F_{fsi} \tag{11}$$

$$I\frac{\partial \omega_i}{\partial t} = T_i \tag{12}$$

$$\frac{\partial \theta_i}{\partial t} = \omega_i \tag{13}$$

where, θ_I is the rotational angle, ω_i the angular velocity, T_i the torque, I the inertia moment, and F_{fsi} the fluid structure interaction. In addition, the center of gravity of a ship hull can be obtained by solving the inertia moment of SPH particles, and this is calculated by using Baraff theory [32]. Therefore, the coordinates of velocity of each SPH particle in every time step can be tracked by using the rotation matrix and the amount of the angle rotation of the center of

gravity. The quaternion is also used instead of the rotation matrix $R(t)$ in 3D to avoid the Gimbal lock phenomenon.

3. Results and Discussions

3.1 Dropping Test of an Elastic Ship

We investigate firstly relationship between elastic motion and impact pressure caused by slamming by conducting a dropping test of an elastic ship. This is simply assumed that water impact load and strain caused by slamming would be obtained from an elastic ship dropping with deadrise angle to still water surface. Here, a model as an elastic ship is the monohull Ferry type. The experiment of the elastic ferry is performed for validating our developed method results in measuring strain which is acting within a deformable ferry model.

3.1.1 Experimental Set Up and Computational Conditions

The experimental set up was determined and designed based on the free fall theory with a constant falling speed. To consider an elastic motion, the ship model is divided into four parts as shown in Fig. 2a. The separated part is connected using a backbone attachment made of metal. The flexural rigidity EI and the ship density are 351 N/m^2 and 243 kg/m^3, respectively. The main dimensions for the actual ship and the model in the experiment are presented in Table 1.

The pressure sensors are located in bow and bottom surface of the model at P1, P2, P3, P4, P5, P6 and P7 and the strains gauges with water proof are located on the backbone attachment at S1, S2 and S3 as shown in Fig. 2b. The Pressure data measured from all points are grouped into three parts, i.e., bow (P_{bow}), hull (P_{hull}) and stern (P_{stern}) to associate with strain data at S1, S2 and S3. Then, high speed video camera with 500 *fps* is placed to capture the ship's motion during the dropping process.

In the experiment, a deadrise angle β of the ship model is defined as a colliding angle between still water surface and an inclined ship at initial condition. Then, the desired angle of the ship model is set and kept with wire before dropping. The deadrise angle β is strictly captured from video image.

For numerical simulation, the dropping test of the elastic ferry has been investigated numerically at the same initial conditions with the experiment as mentioned above. The Ferry model is represented by a large number of the SPH particles where the radius of the SPH particle is 0.0025 L_{pp} and the total number is 29,434. The grid size is 0.01 L_{pp} and the radius of free surface particle is 0.0025 L_{pp} and the total number located near the free surface is 127,680. The density ratio between air and water is 800 and the viscosity ratio between them is 55 in the multiphase model. The flexural rigidity *EI* and the ship density are 351 Nm^2
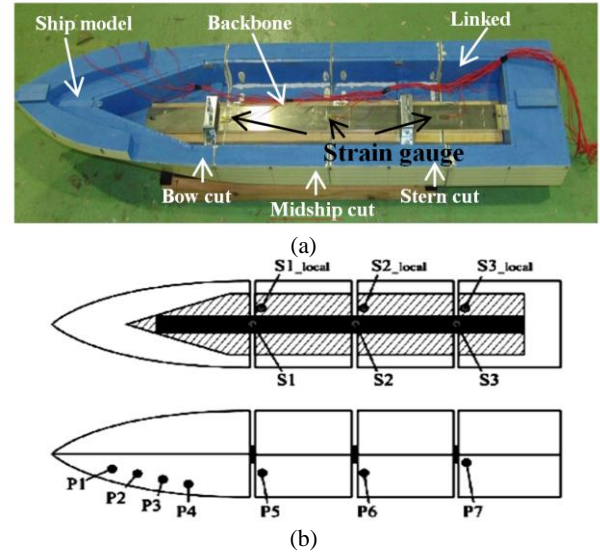

(a)

(b)

Fig. 2 (a) Ship model; (b) Location of pressure sensors and strain gauges.

Table 1   Main dimensions of actual ship and model.

	Actual ship	Model
Loa (m)	45	1.5
B (m)	9.6	0.3
H (m)	3.5	0.116
T (m)	1.2	0.04

and 243 kg/m^3, respectively. The initial dropping speed is used about 4.4 m/sec recorded by high-speed video camera in the experiment.

3.1.2 Comparison Results

Fig. 3 shows comparison of typical case of the elastic behavior and the free surface based on some snapshots between the experimental and the numerical results during the dropping and the entering process for deadrise angle β two degrees. Vertical location of the elastic ship, water splashing and free surface deformation change at each time step from 0.001 sec to 0.03 sec, as shown in that figure. From the comparison, the numerical result is quite good agreement with the experimental one. However, there
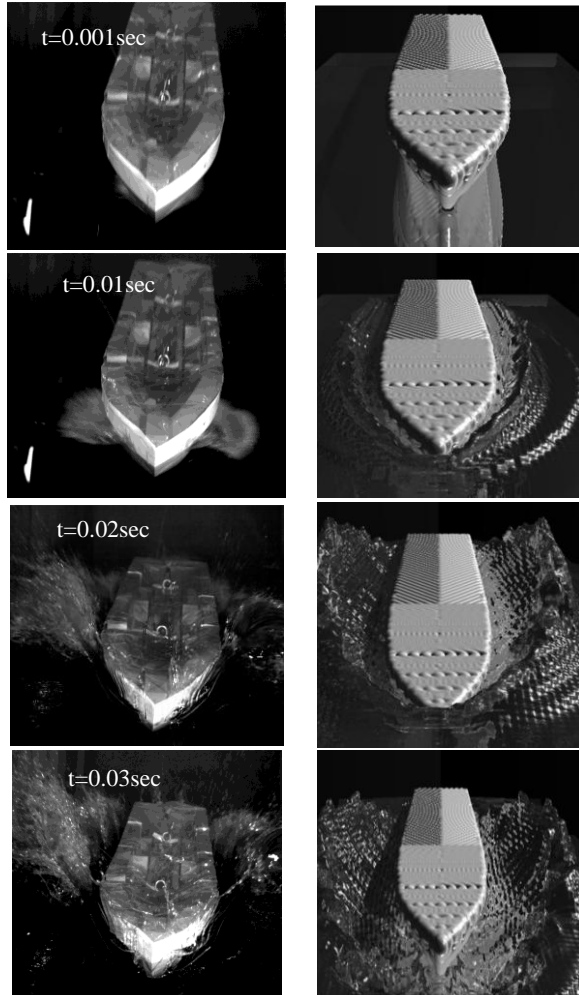

Fig. 3   Comparison typical case of the elastic behavior and the free surface for $\beta = 2°$.

is small discrepancy between them during the entry process. When the ship bow contacted firstly on the water surface and then immersed, the water splashing near the bow and the generated short wave reflection along the ship are comparatively weak in the numerical results because small droplets and air bubbles less than the size of the free surface particles cannot be captured by our numerical model. The present model need to overcome this problem using another special technique in near future work.

In our previous numerical result, the computed result of an elastic rectangular body with deadrise angle was compared with the experimental result in pressure and strain and its result is in good agreement with our experimental results [25]. In present study, we need to focus on strain caused by impact pressure due to ship slamming and validate the strain with the experimental data.

Fig. 4 shows an example comparison of the strain time histories between numerical and experimental results for deadrise angle $\beta = 2°$ at S1, S2 and S3, respectively.

The numerical result is quite good agreement with the experimental result. However, the strain histories at S2 have a little discrepancies between computational result and experimental one. The strain at the stern part is caused by strongly interaction between the elastic ship model and the free surface with splashing during the elastic behavior response to the water.

Moreover, the impact pressure was distributed on the ship surface during the entry process as shown in Fig. 5. The high impact pressure is firstly occurred at the bow part when the ship just touched on the free surface. The high impact pressure region are also generated on the bow and midship parts at 0.02 s to 0.03 s. This indicates that the impact pressure is occurred by the strongly nonlinear slamming phenomena. For design analysis, the bow flare and the ship form would become important factor to avoid and reduce effects of slamming.

(a) Location S1   (b) Location S2
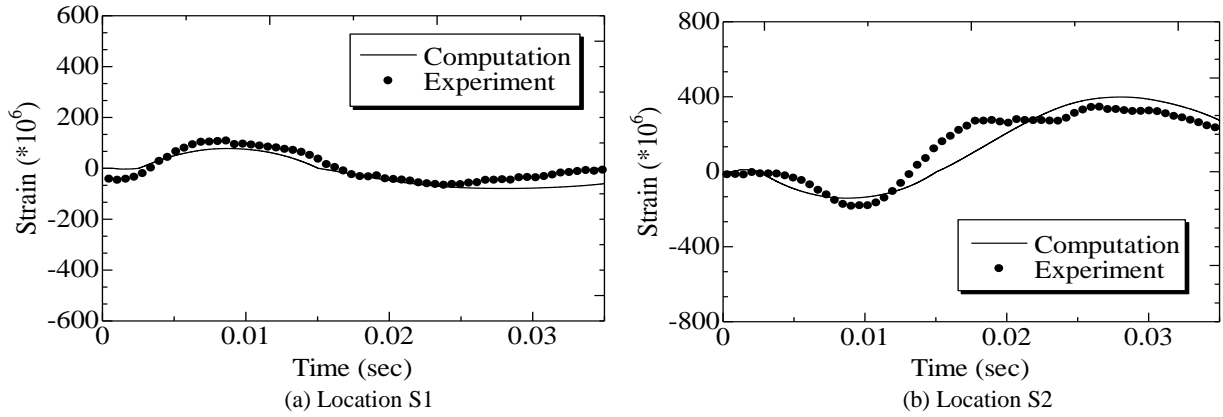
Fig. 4   Comparison of the strain time histories between numerical and experimental results at S1 and S2 for $\beta = 2^{o}$.

Front view   Bottom view

(a)   t = 0.01s

(b) t = 0.02s

(c) t = 0.03s

$P*$

100   500
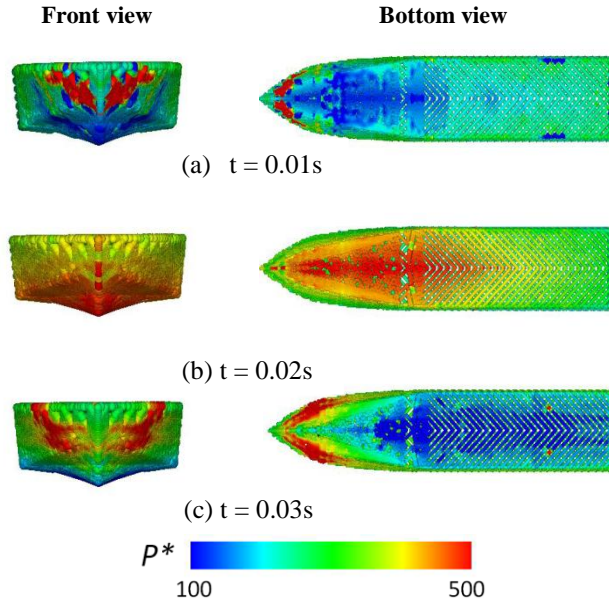
Fig. 5   Ressure distribution on ship surface during the entry process.

Based on the comparison results, the hybrid particle-grid scheme is acceptable to be used for investigating interaction between elastic ship motion and wave. In the following section, using the developed method, we have investigated on elastic ship motion in nonlinear wave with breaking under slamming event to be obtained and clarified some effects of hydroelastic behaviors.

3.2 Investigation of an Elastic Ship Motion in Nonlinear Wave

In this section, the investigation is emphasized to analyze hydroelastic behaviors under slamming by

applying our numerical method to ship motion in heading regular wave with breaking. The main dimensions of a ship which are used in this section is the same with those of the dropping test as explained in previous section.

3.2.1 Computational Conditions

In the computational conditions, the F_n are set to 0.32 and 0.45. Then, Reynolds number is about 1.4×10^6. Young's modulus is 210 GPa and Poisson ratio is 0.3 for the elastic ship. The incident wave height H_w/L_{pp} is 0.06, L_{pp} is a ship length and 12 cases are performed based on the different wave length λ and the ship speed V. The grid size dx, dy and dz are 0.01

L_{pp}. The radius in both free surface particle and SPH particle are 0.0025 L_{pp} and the number of particle is 542,000 for free surface and 29,306 for elastic ship (SPH particle).

The impact pressure acting on the ship can be monitored and recorded in time evolution. Then, each SPH particle produces the strain in six components based on three dimensions in local axes of SPH method, i.e., *xx*, *xy*, *xz*, *yy*, *yz* and *zz*. Two measuring points of pressure, P1 and P2 as shown in Fig. 6, are located on the ship bow and bottom, respectively. Then, three measuring points of strain, S1, S2 and S3, are located on along deck as shown in Fig. 6. The P1 is represented by bow slamming and P2 is bottom slamming. The strain measuring points at S1, S2, and S2 are characterized by the deck structure in front, mid and rear parts, respectively.

3.2.2 Results and Discussions

Fig. 7 shows example of time history of the computed pressure measured at bow part P1 and bottom part P2 for F_n = 0.32 and L_{pp}/λ = 0.2. From those figures, the pressure at P1 is periodically higher than P2. This means that the bow slamming is occurred with high pressure and the localized impact pressure can result substantial damage on bow flare of the ship. Fig. 8 shows the typical non-dimensional

(a) Side view

(b) Bottom view

(c) Top view
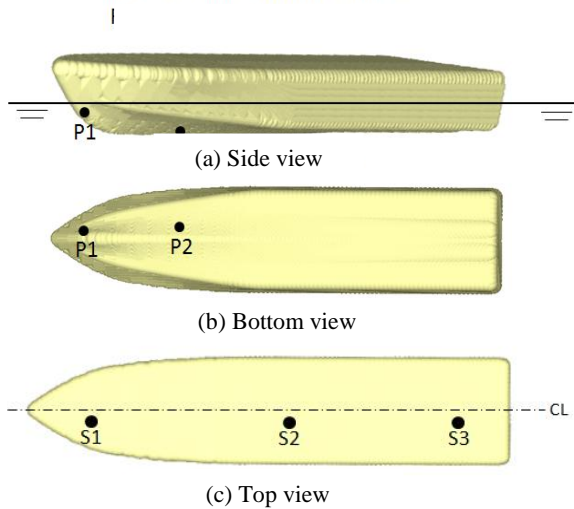
Fig. 6   Location of measuring points of pressure and strain.

(a) P1 moving average)

(b) P2 (moving average)
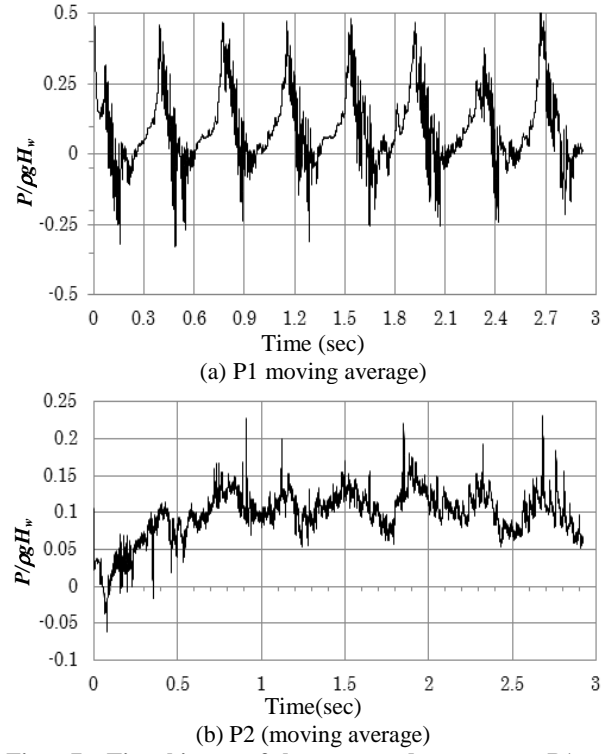
Fig.   7   Time history of the computed pressure at P1 and P2 for F_n = 0.32.

impact pressure defined by averaging maximum pressure *P** each case in increasing wave length L_{pp}/λ for both cases F_n = 0.32 and 0.45 where it is nondimensionalized by wave height H_w, water density ρ and gravity acceleration *g*.

The localized impact pressure shows the same tendency in all cases based on F_n. It increases when the ship speed increases and is higher at bow part P1 about four times than at bottom part P2. Then, the localized impact pressure tends to increase with increasing wave length, however, it gradually decreases when the L_{pp}/λ is greater than or equal to 1.0. This can be notified that L_{pp}/λ = 1.0 is critical point for bow slamming. Fig. 9 shows some snapshots of bow slamming and bottom slamming phenomena during the motion in nonlinear wave with breaking. The ship's bow hits the surface of wave crest and it is then categorized by bow slamming event and the bottom slamming event that bottom of the ship is lifted up and reenter into free surface due to the loading as shown in Fig. 9. In addition, the wave breaking
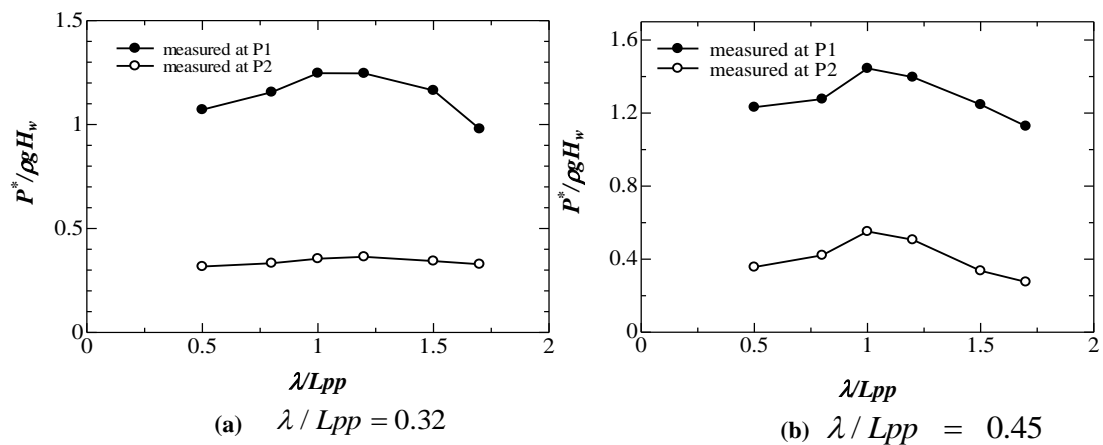
Fig. 8   Typical localized impact pressure acting on bow and bottom parts.
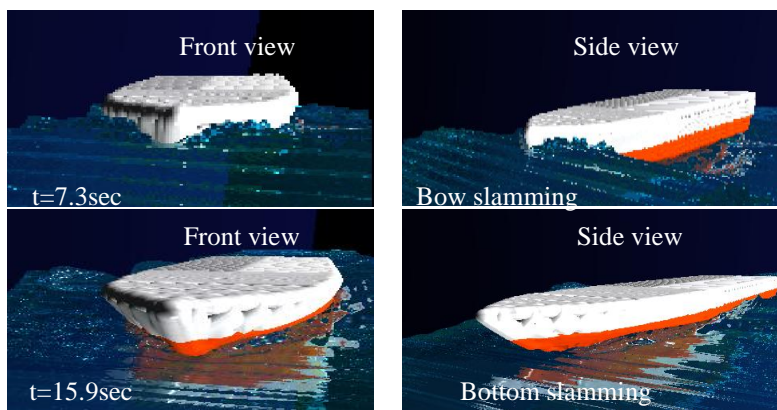
Fig. 9   Snapshots of bow slamming and bottom slamming with breaking.

can be captured well.

The ship experienced strain after the impact pressure acted to the ship. It was bended upward and downward.

The reaction of strain on the deck that causes the bended ship is shown in Fig. 10. The localized strains S1, S2 and S3 grow up with increasing wave length.
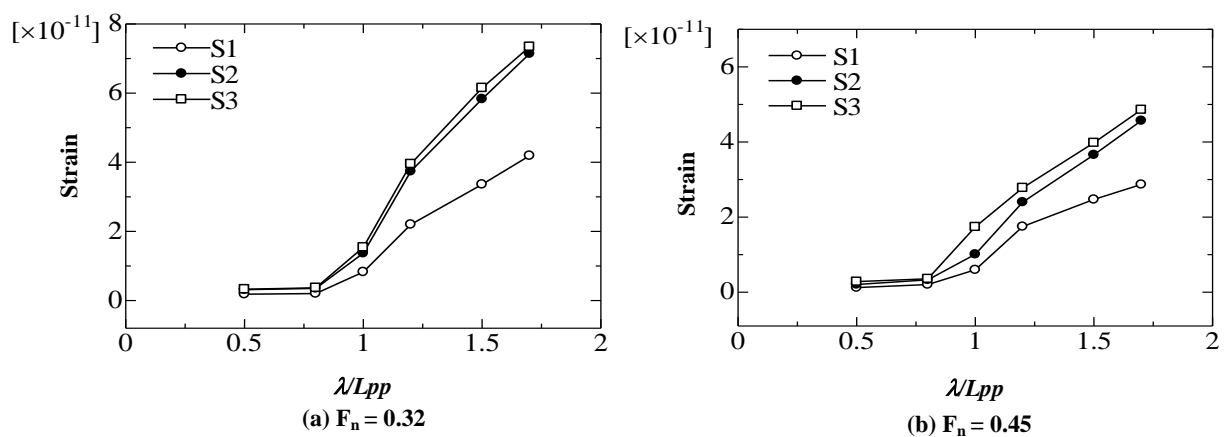
Fig. 10   Typical localized strain response reacting on deck caused by hydroelastic behavior.

This means that the impact pressure is low as shown also in Fig. 8 where the impact pressure tends to decrease when $L_{pp}/\lambda \geq 1.0$. In addition, the localized impact pressure measured at S3 is highest in both cases based on Fn. The shape of the stern has a slightly flat of hull and a small draft, consequently these can contributes high strain. In future study, we will investigate local strain on along keel part.

When wave load is applied, the shape of the ship could suffer hogging and sagging. This has been also explained previously. Fig. 11 shows the non-dimensional global impact pressure P^* acting on the ship normalized by density ρ, gravity acceleration g and wave height H_w. High speed influence an magnitude of global impact pressure as shown in Fig. 11. The high global impact pressure occurs when $L_{pp}/\lambda = 1.0$ and this is reasonable that the level wave load as show in Fig. 8 is highest. Moreover, the shape of hogging and sagging are completely described when the wave is the same length with the ship $L_{pp}/\lambda = 1.0$. Hogging that ship is where the crest of the wave is in amidship and sagging that ship is in the trough of two waves.

The global impact pressure is rarely investigated than the localized impact pressure. In fact, a mid of a ship is vulnerable to some disturbances due to loading because it can cause snap or crack. Therefore, in each case based on wave length, the high deflection of vertical bending load is defined at the centre gravity of the ship.

Fig. 12 shows the nondimensional vertical bending moment defined at the centre gravity of the ship. It can be seen also that high speed contributes strong bending moment because heave amplitudes of the ship becomes large. The vertical bending moment grows up in increasing the wave load level hereafter it tends to decrease about two times the ship length. This depends on a ship position related with that wave crest and trough even though a wave length is bigger or equal to two.

Furthermore, comparison the nondimensional heave and pitch amplitudes between elastic ship and solid ship is show in Fig. 13.

The nondimensional pitch and heave amplitudes are defined by Hv/Hw and $\theta a/(H\_w*k)$, where, Hv is heave motion amplitude, Hw the wave amplitude, θa the pitch motion amplitude and k the wave number.

Based on the comparison result of the nondimensional heave amplitude, the heave amplitude of elastic ship is lower than solid ship in each wave length. In contrary, the nondimensional picth amplitude of the elastic ship is higher than the solid one. In addition, high Fn contributes large amplitude for the elastic case. Here, this can be seen significantly that ship motions are also influenced by hydroelasticity behaviors. Therefore, the performance of a ship in nonlinear wave with breaking depends on impact pressure, elastic structure and ship speed.
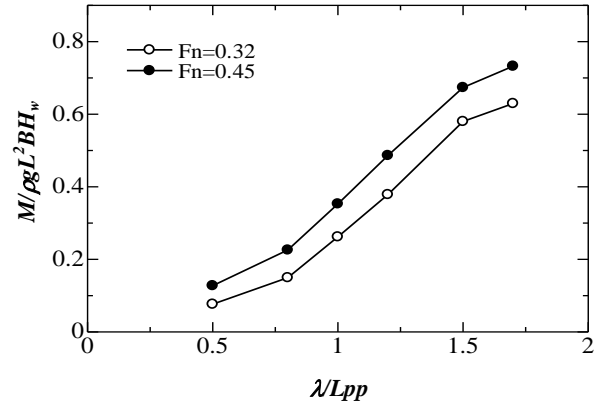
Fig. 11   Nondimensional global impact pressure acting along the ship for F$_n$=0.32 and F$_n$=0.45.
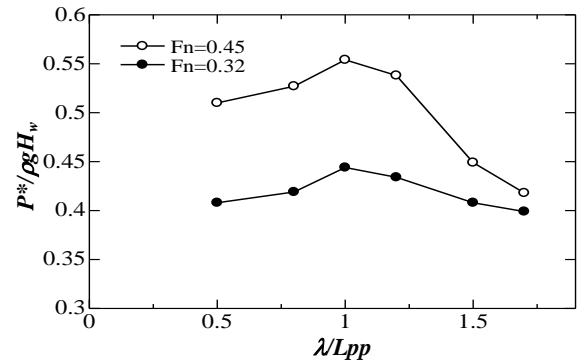
Fig. 12   Nondimensional vertical bending moment defined at centre gravity caused by global impact pressure.
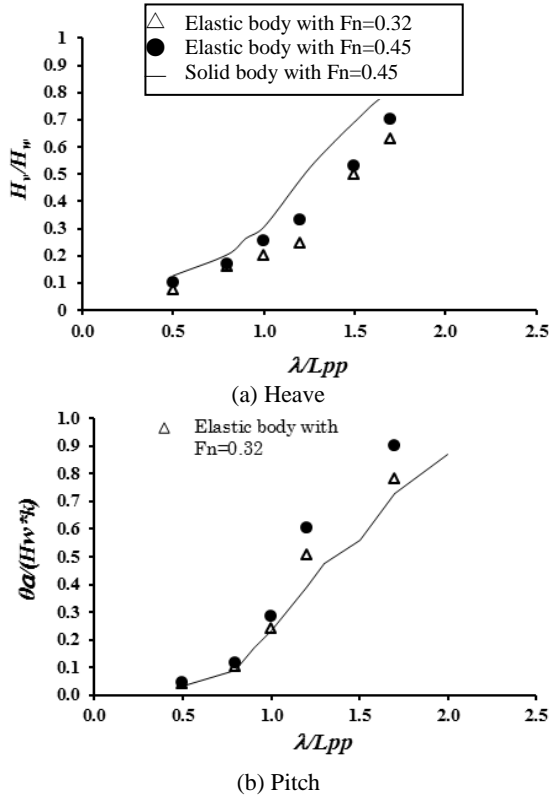
(a) Heave

(b) Pitch

Fig. 13   Comparison of the nondimensional heave and pitch amplitudes between solid and elastic bodies.

4. Conclusions

In the present study, the hybrid particle-grid scheme has been developed to investigate hydroelastic effects on both the dropping test of the ship and ship motion in nonlinear wave with breaking.

From the dropping test of the ship, the numerical result of vertical location of the elastic ship during the falling, water splashing and free surface deformation and strain history are overall in quite good agreement with the experimental results. However, there is small discrepancy between them during the entry process. These numerical errors were caused by small water droplets and air bubbles less than the size of the free surface particles.

The performance of a ship in nonlinear wave with breaking is influenced significantly by hydroelastic behaviors of the ship. These can be seen that hydroelastic effects address directly to impact pressure

and vertical bending moment. The high F_n contributes large amplitude in both motion and bending moment for the elastic case. Here, this can be seen clearly that ship motions are also influenced by hydroelasticity behaviors. Therefore, the performance of a ship in nonlinear wave with breaking depends on impact pressure, elastic structure and ship speed.

The all result of the investigation of elastic ship motion in nonlinear wave with breaking by using hybrid particle-grid scheme needs to be validated with experimental work. Hence, in future work we will conduct experiment of an elastic ship motion in wave. Moreover, the size of the free surface particle will be considered also to capable handle a small water droplet and air bubble resulted by strongly interaction wave-ship.

Acknowledgments

References

[1] Inglis, C.E., Natural frequencies and modes of vibration in beams of non-uniform mass and section, Trans. R. Instn. Nav. Architects 72 (1929) 145-166.

[2] Heller, S.R., Abramson, H.N., Hydroelasticity–A new naval science, J. Am. Soc. Nav. Engrs. 71 (1959) 205-209.

[3] Bishop, R.E.D., Price, W.G., Hydroelasticity of Ships, Cambridge University Press, London, 1979 p. 423.

[4] Von Karman, T., The impact of seaplane floats during landing, NACA, TN321, Washington (1929).

[5] Wagner, H., Uber stoss-und Greitvergange a der Ober-flache von Flussigkeiten, Zeitschr. F. Angrew. Math. Und Mech. 12 (4) (1932) 193-235.

[6] Chuang, S.L., Experiment on slamming of wedge-shaped bodies, Journal of Ship Research 11 (1967) 190-198.

[7] Greenhow, M., Lin, W.M., Nonlinear Free Surface Effects: Experiment and Theory, Report No.83-19, Dept. of Ocean Engineering, MIT, 1983.

[8] Greenhow, M., Water entry into initially calm water, Applied Ocean Research 9 (1987) 214-223.

[9] Eagle, A., Lewis, R.A., A comparison of hydrodynamic impacts prediction methods with two dimensional drop

test data, Marine Structure 16 (2003) 175-182.

[10] Zhao, R., Faltinsen, O.M., Water Entry of two-dimensional bodies, J. Fluid. Mech. 246 (1993) 593-612.

[11] Zhao, R., Faltinsen,O.M., Aarnes, J., Water entry of arbitrary two-dimensional sections with and without flow separation, in: Proc. of 21st Symp. on Naval hydrod ,1997, pp. 408-423.

[12] Zhao, R., Faltinsen,O.M, Water entry of arbitrary axisymmetric bodies with and without flow separation, in: Proc. of 22nd Symp. On Naval hydrod, 1998, pp. 652-664.

[13] Faltinsen, O.M., The effect of hydroelasticity on ship slamming, Phil. Trans. R. Soc. 355 (1997) 575-591.

[14] Faltinsen, O.M., Hydroelasticity of high-speed vessels, hydroelasticity in marine technology, in: Proc. of the 2nd international Conference, 1998, pp. 1-13.

[15] Bereznitski, A., Boon, B., Postnov, V., Hydroelastic formulation in order to achieve more accurate prediction of hydrodynamic loads, in: Proc. of 11th International Offshore and Polar Engineers Conference, 2001, pp. 337-342.

[16] Bereznitski, A., Postnov, V., Hydroelastic model for bottom slamming, in: The 8th International Symposium on Practical Design of ship and Other Floating Structure, China 2 (2001b), pp. 911-917.

[17] Bereznitski, A., Kaminski, M.L., Practical Implications of Hydroelasticiy in Ship Design, in: Proc. of 11th International Offshore and Polar Engineers Conference [CD-ROM] (2002).

[18] Bereznitski, A., Boon, B., Postnov, V., The effect of hydroelasticity on the impact pressure due to bottom slamming on ship structure, in: Proc. of 11th International Society Offshore and Polar Engineers Conference IV, 2002, pp. 227-283.

[19] Tajima, M., Yabe, T., Simulation on slamming of a vessel by CIP method, J. of the Phys. Soc. of Japan 68 (8) (1999) 2576-2584.

[20] Watanabe, I., Takemoto, H., Miyamoto, T., Use of an elastic model in studying wave loads on a ship in waves and its verification by a full-scale measurement, in: Proc. of the International Symposium on Scale Modeling, Japan Society of Mechanical Engineers, 1988, pp. 47–55.

[21] Faltinsen, O. M., Water entry of a wedge by hydroelastic orthotropic plate theory, Journal of Ship Research 43

(1999) 180-193.

[22] Faltinsen, O.M., Slamming with application to planning vessels, green water loading and sloshing, Hydrodynamics in Ship and Ocean Engineering (2001) 27-58.

[23] Senjanovic, I., Malenica, S., Tomasevic, S., Investigation of ship hydroelasticity, Ocean Engineering 35 (2008) 523-535.

[24] Thomas, G. et al., Slam events of high-speed catamarans in irregular waves, Journal Mar. Sci. Technol. 16 (2010) 8-21.

[25] Baso, S., Mutsuda, H., Kurihara, T., Kurokawa, T., Doi, Y., Shi, J., An Eulerian scheme with Lagrangian particles for evaluation of seakeeping performance of a ship in nonlinear wave, International Journal of Offshore and Polar Engineering 21 (2) (2010) 103-110.

[26] Baso S., Mutsuda, H., Kawakami, K., Hashihira, K., Doi, Y., Numerical study on nonlinear hydroelastic and hydrodynamic effects on floating body using eulerian scheme with lagragian particles, in: Proc. of the 21st International Society Offshore and Polar Engineers Conference, 2011, pp. 610-617.

[27] Yabe, T., Mizoe, H., Takizawa, K., Moriki, H., Hyo-Nam Im, Ogata, Y., Higher-order scheme with CIP method and adaptive soroban grid towards mesh-free scheme, Journal of Computational Physics 194 (2004) 57-77.

[28] Gingold, R.A., Monaghan, J.J., Smoothed particle hydrodynamics, theory and application to non-spherical stars, Mon. Not. Roy. Astr. Soc. 181 (1977) 375-389.

[29] Mutsuda, H., Yasuda, T., Numerical simulation of turbulent air-water mixing layer within surf-zone, in: Proc. of the 27th International Conference on Coastal Engineering, 2000, pp. 755-768.

[30] Takewaki, H., Yabe, T., Cubic-interpolated pseudo particle (CIP) method application to nonlinear or multi-dimensional problems, Journal of Computational Physics 70 (1987) 355-372.

[31] Mutsuda, H., Doi, Y., Numerical simulation of dynamic response of structure caused by wave impact pressure using an eulerian scheme with lagrangian particles, in: Proc. of the 28th International Conference on Ocean, Offshore and Arctic Engineering, [CD-ROM] (2009).

[32] Barraf, D., An introduction to physically based modeling, Rigid body simulationI ~Unconstrained rigid body dynamics~, SIGGRAPH'97 course note D3 (1997).

Scrap Activities on the Coastal Zone: Dynamic Model for the Recycling of Ships

Aristotelis B. Alexopoulos

Department of Shipping, Transport and Logistics, BCA College Poseidonos & Fivis, Athens 16674, Greece

Abstract: This paper describes the main activities of the ship recycling facilities that have moved to the Asia continent and puts emphasis on environmental and working conditions under the umbrella of the new IMO (International Maritime Organization) convention. However, the convention is not enforced yet and the legal gaps found on limited existing regulations do not impose strict rules on the shipping industry and at the same time offer motives for the safe recycling of ships. Ship-owners seem reluctant to send their vessels for scrap but rather prefer to employ them till the last minute, preferably in areas where the environmentally-friendly concept is not of primary importance. The dynamics of this specialized industry can be better shown by examining variables such as legal instruments, occupational health and safety hazards, geographical allocation of scrapping sites, scrap prices, safety working plans and volume to be scrapped. The next step is to build a simulation model in order to discuss the relevant scenarios. The first scenario is based on the current conditions where the ship-owner's decision is mainly affected by the fluctuations of the market and whether the effectiveness of existing regulations can improve the working environment in terms of health and safety. The second scenario refers to the situation when the IMO Convention is implemented, then it will produce two major recycling markets, the first one for the convention ships and the second for non-convention ships.

Key words: Ship recycling, health and safety, IMO Hong Kong Convention, system dynamics.

1. Introduction

Ship recycling, as one of the basic principles of sustainable development, is the most environmentally friendly procedure of dismantling ships since every part of the hull and machinery can be re-used. Ship dismantling is the result of ship breaking for scrap or disposal of a vessel's structure irrespective where it is conducted, i.e., at a beach, pier or dry-dock [1]. It includes a wide variety of actions, from removing all components and equipment to cutting down and recycling its infrastructure.

However, ship breaking is a very hazardous occupation on account of many environmental, safety and health issues involved, that nowadays has been concentrated in some developing nations (mainly in Asia). Yet, even if ship recycling is the beneficial

result for handling ship scrapping, the global picture is not optimistic, mainly because environmental standards and working practices in recycling facilities are quite poor [2]. So far, there is a lack of specific prescriptive requirements in the existing regulatory instruments dealing with ship breaking and ship recycling matters [3]. However, the IMO has adopted the HKC (Hong Kong Convention) on ship recycling in 2009, though it is not yet in force.

At the moment, without mandatory regulations ship-owners seem quite reluctant to enforce stringent practices for prevention of marine accidents and marine pollution when sending the vessel to her last voyage, let alone many states prefer the enforcement of national regulations/rules for their scrapping/recycling industries (several decisions in European courts, i.e., France, Norway, Belgium).

In this study, we have analyzed the main key-drivers that may affect the ship-owner's decision to send his vessel for scrap, such as the chartering and

Corresponding author: Aristotelis B. Alexopoulos, Ph.D., research fields: marine environmental law, coastal zone management, international maritime regulations, shipping policy and ship management. E-mail: aalexopoulos@bca.edu.gr.

ship-recycling markets, the operational costs, the existing regulations and the supply of vessels for scrap. Then, we have used the system dynamics methodology to develop a mathematical model that is presented as a stock-flow diagram that captures the model structure and the interrelationships among the variables. This diagram is translated to a system of differential equations and then numerically solved via simulation. In this paper, the model has been built using the Vensim® PLE software package developed by Ventana Systems, Inc., The model focuses on the presentation of two categories of states that offer scrap service, the first group consists of states that are fully complying with existing regulations offering competitive scrap prices and the next group of states which offer higher scrap prices with low working safety and health levels. This distinction will assist in determining the ship-owner's choice for a recycling yard in view of the regulations.

2. Overview of Ship Recycling

Ships are mobile structures of sometimes enormous size that consist mainly of steel. At the end of their operational life, they become obsolete and sources of ferrous scrap. Instead of being scuttled, or used as artificial reefs or even worse in some rare cases as floating waste reception facilities, they should be demolished and recycled. The obvious benefits of such operations are a useful source of supply for second hand equipment and components, particularly for the developing states that depend their economy on such products, and above all a contribution to sustainable development (steel is recycled at much lower cost than importing and processing iron ore and less energy is needed).

The importance of dismantling ships as potential sources of raw material for importers was recognized in the early 1970s. At that time, the centre of scrapping industries were U.S. and Europe, particularly in Spain (Cadiz was the main port for scrapping). Work was carried out at docks by skilled

personnel but the increasing cost of upholding health and safety regulations made it non-profitable. In the beginning of 1980, a shift to the Asian region was seen, notably Taiwan followed by South Korea became receivers of decommissioned tonnage due to low labor costs and the absence of obligatory regulations for safe working environments [4].

In the early 1990s, China became the new centre for scrapping ships but she proceeded with the introduction of taxes on tonnage imported for scrap. Nowadays more than 90% of the scrapping operations, representing some 58% of the annual number of ships scrapped, take place on the beaches of Bangladesh (Chittagong), India (Alang), Pakistan (Gaddani estate in Baluchistan) and in China[1]. For these states, scrapping operations have certain impacts on local community because of the volume of scrap to be removed that generates employment and revenue for local economy and due to low operating costs since they are a perfect market for the scrap components.

After 25-30 years, more or less ships reach the end of their lives. Hundreds of vessels are sent to scrap each year (about 600 to 700) and it is estimated that this trend will continue mainly because: (1) New regulations are brought up that update ship-designs[2] and (2) the phasing-out schedule of single-hull tankers according to MARPOL's (Marine Pollution convention) provisions creating a matter of capacity[3]. Some states put pressure to enhance this schedule so

---

[1] The re-entry of China as a major scrapping nation should be regarded as an exception because she is investing in the improvement of scrapping methods by introducing new technologies, www.ban.org/Library/shipbreaking_china.html (October 24, 2006).

[2] A new approach to ship construction from the legal point of view is the GBS (Goal-Based Standards) that was introduced in IMO (2002) through a proposal by Greece and Bahamas, stating that IMO should play a larger role in determining the standards to which new ships are built, traditionally the responsibility of classification societies and shipyards. See IMO News, No. 1, (2006), 13-17.

[3] On 5 April 2005, a revised schedule for the phasing-out of single-hull oil tankers and a new regulation banning the carriage of heavy grade oil in single-hull oil tankers entered into force (as amendments to Annex I of MARPOL following the sinking of the Prestige off the Spanish coast). See IMO News, No. 2, (2005), 6-7.

more of them will resort to scrapping by beaching.

Each year, almost 700 vessels of over 2,000 dwt are being dismantled worldwide. In 2010, a peak occurred owing to the phasing-out of 800 single-hull tankers, according to MARPOL's provisions [5]. More than 2/3 of those ships were scrapped and/or recycled on the South-Asian beaches. Pressure was put to the IMO by some member-states to enhance the phasing-out schedule, so more vessels would resort to scrap by beaching, i.e., the critical date for pre-MARPOL tankers was brought forward from 2005 to 2007 and for MARPOL tankers from 2010 to 2015[4].

However, the key-statistics is the size of the operating world fleet because it is affected by new-buildings, old ships sent for scrapping and/or recycling and various ship casualties. In addition, by examining statistical databases on ship recycling we must bear in mind that, the available data suffer from discrepancies [6], i.e., many ship-owners do not always report how many ships are recycled or they only have reported them a considerable time after they were recycled (some ships though stated as recycled they are found to be operating and/or trading). Consequently, data published for one or more years must be revised.

It is worth noting that, there is a cyclical tendency of the recycling market with low volumes in recent times. This is also justified by the figures on the average age of ships sent for scrap, from 26-27 years old in the previous decade to around 32 years old at present. The basic cause for this picture is the fluctuations in the freight market in most shipping sectors, primarily the earnings for tankers and bulk carriers (that remained in the market because the economics of their operation dictated it).

It is obvious that low volumes of ship recycling are explained by the high recycling prices. We may assume that there is a connection between freight market rates and recycling prices but not only that,

since another important factor that drives the recycling prices is the local demand for ship parts in each recycling market, particularly the South-Asian ones.

The differences in prices reflect differences in labour and environmental costs for recycling ships as well as the different local demand for steel, i.e., Bangladesh derives 80%-90% of its steel from end-of-life ships (if there is a slowdown in the shipbuilding industry demand for steel will drop and ship-breaking yards are directly affected). Also, ship-owners with small-sized ships prefer the Turkish market since the lower lightship does not cover their costs through the Suez Canal for longer voyages to India, Pakistan, etc. [7].

To this, we may note the major difference in labor costs between Asia and Europe. While workers on demolition sites in Bangladesh and India earn 1-2US$/day and employers' expenses for safety and health are negligible, the costs in Europe are estimated at around 250US$/day for a worker in Netherlands and 13US$/day in Bulgaria [8]. All these differences in labor costs, environmental and health requirements, and revenue from recycling and second-hand materials explain why operators in South Asia offer much better prices to ship-owners than their European competitors.

It is true that the recycling industry eliminates obsolete and substandard ships, and therefore it is the key element of maritime safety and environmental protection and of economic balance in the shipping markets. The more expensive it is to recycle a ship, the later it will be sent for scrap and the higher it will be the average second-hand ship's age of the world's fleet. The remaining of older ships in the market will obviously depress it and increase substantially the risks of loss of life and accidental pollution. This will mean even higher hazards for the maritime safety. As a result, no matter what constitute authorities and maritime industries do in order to deal with hazardous materials, the recycling procedures can better be controlled at the recycling facilities.

---

[4] Regulation 13G amendments of 2003 (phasing out schedule) after the disaster of Erika in the French coast in 1999.

3. Legal Implications Related to the Recycling of Ships

The issue of ship recycling was firstly introduced at the IMO in 1998 and 4 years later, based on a work plan on ship recycling it was decided to develop a recommendatory instrument which would take into account the following documents:

• Industry Code of Practice on Ship Recycling (2001);

• Guidelines of the Basel Convention for ship recycling facilities (1989);

• Guidelines of the ILO (International Labour Organization) which refer to working conditions at recycling facilities (2004);

• Council regulation 259/93/EEC on the supervision and control of shipments of waste within, into and out of the European community (1993).

3.1 IMO's Initiatives

The IMO "Guidelines on Ship Recycling" were adopted in 2003 by Resolution A.962(23) and further modified in 2005 by Resolution A.980(24). The main concept of the guidelines is that nothing, in the process of recycling, is wasted, i.e., steel is reprocessed, generators are re-used in shore industries, batteries are absorbed by the local economy, hydrocarbons become reclaimed oil products, etc.. However, the guidelines recognize that there should be paid greater attention to the working practices and environmental standards in these facilities.

Furthermore, in order to prepare the ship for the dismantling process and all material on board to be handled safely and properly, a document called "Green Passport" should accompany the vessel during its operating life [9]. This is prepared by the shipyard for new ships whereas for existing ships it's the ship-owner's responsibility. However, a recycling facility should be selected based on its capability to recycle the vessel according to existing national and international regulations. In particular:

• "Technical Guidelines for Environmentally

Sound Management" in ship dismantling facilities, developed by the Joint Working Group of ILO/IMO/ Basel Convention [10]. According to the Basel Convention, a special section refers to ship dismantling that safeguards those employed in it and protects the environment while recognizing the role the industry plays in the economies of some developing states.

• "Guidelines on Safety and Health in Ship-breaking" developed by ILO. They refer to Asian countries and Turkey and are designed to assist ship-breakers and competent authorities to implement the ILO standards on occupational safety and health. The guidelines present details on the safe conduct of ship-breaking operations, e.g., planning, safety requirements, management of hazardous substances, etc. [11].

Also, the "Guidelines for the Development of the Ship Recycling Plan" were introduced in 2004 by the IMO. The dismantling of a ship should be executed according to this plan defined by both the ship-owner and the recycling facility. It must comprise of three main parts:

• SHP–A worker safety and health plan. It contains procedures for protecting worker's health and safety.

• ECP–An environmental compliance plan. It is an evaluating tool so that the recycling facility acknowledges the environmental risks associated with ship recycling and can manage and dispose of all materials used from the ship's structure in an environmentally sound manner.

• OP–An operational plan. It describes the technical issues to performing the work, focusing on procedures to handle hazardous materials with success and ensure compliance with applicable worker safety.

3.2 The Hong Kong Convention on Ship Recycling

IMO adopted the convention for the Safe and Environmentally Sound Recycling of Ships, held in Hong Kong (2009) which aimed at ensuring that ships, when being recycled after reaching the end of their

operational lives, do not pose any unnecessary risk to human health and safety or to the environment. However, the convention is not yet in force (until October 31, 2011, no member-state has signed it). It needs the signature or ratification of 15 states representing 40% of world merchant shipping by gross tonnage [12].

The HKC deals with ship recycling issues and puts emphasis on (1) ships sold for scrap that may contain environmentally hazardous substances such as asbestos, heavy metals, hydrocarbons, ozone-depleting substances and others, and (2) problems related to the working and environmental conditions in ship recycling locations. Ships sent for scrap are required to carry an "inventory of hazardous materials", which will be specific to each ship. In parallel, ship recycling yards will be required to provide a "ship recycling plan", to specify the manner in which each ship will be recycled, depending on its particulars and its inventory.

Apart from the articles, annexes and appendices the new convention includes specific guidelines establishing uniform procedures for technical issues stemming from its basic provisions. These guidelines are two-folded[5].

• Guidelines for ships: development of inventory of hazardous materials, surveys and certification, inspection of ships, and establishment of gas-free-for-hot-work conditions.

• Guidelines for recycling facilities: authorization of

---

[5] The following guidelines have been developed and adopted to assist States in the early implementation of the Convention's technical standards: (1) 2011 Guidelines for the Development of the Ship Recycling Plan, MEPC.196(62) and (2) 2012 Guidelines for the Safe and Environmentally Sound Ship Recycling, MEPC.210(63). Also two further guidelines have been developed and adopted to assist states in the implementation of the convention after it enters into force: (1) 2012 Guidelines for the Survey and Certification of Ships under the Hong Kong Convention, MEPC.222(64) and (2) 2012 Guidelines for the Inspection of Ships under the Hong Kong Convention, MEPC.223(64).

ship recycling yards, safe and environmentally sound ship recycling, development of ship recycling plan.

However, the HKC is under heavy criticism mainly because:

(1) It ignores the basic principles under the Basel Convention. According to this convention the export of hazardous wastes has been banned for any reason, including recycling from 1998.

(2) It fails to demand for de-contamination of ships in developed states prior to the final export. According to Council Regulation 259/93/EEC on the "Supervision and Control of Shipments of Waste within, into and out of the European Community (1993)", the scrapping of OECD (Organization for Economic Co-operation and Development) tonnage outside the OECD area is subjected to Basel Convention regulations. Many European states consider end-of-life ships as "waste" that need to be de-contaminated prior to export.

(3) It limits state responsibility to minimum requirements and only places those on flag states and ship-breaking states. However, another view expressed is to avoid excessively binding standards that cannot be applied worldwide and refrain a state from signing and ratifying the convention.

(4) It exempts military and government ships (although all IMO existing conventions provide for the same exception, this is a very delicate issue that should be re-considered). Thousands of ships are built with toxic substances such as asbestos and PCBs (Printed Circuit Boards). In the Clemenceau case, a defunct aircraft carrier laden with asbestos and PCBs, was exported by the French government to India only to be called back after a French court ruled that France, in exporting the vessel, was not abiding by the rules established under the Basel Convention and Council Regulation.

3.3 The UN Basel Convention

The UN Basel Convention on the control of trans-boundary movements of hazardous wastes and

their disposal was adopted in 1989. The overall goal of the convention is to protect human health and the environment against adverse effects which may result from the generation, management, transboundary movements, and disposal of hazardous wastes. It is relevant for ship dismantling, as a ship that is sent for scrapping usually contains hazardous materials and may, therefore, be considered as a shipment of hazardous waste. Thus, it applies to all ships which are "waste" as defined by the convention. There are no exceptions for any types of ship [13].

The principle of environmentally sound management of hazardous waste is a central goal, applying to all facilities that recover or dispose of waste. Ship recycling facilities shall be authorized in accordance with the convention's principles of ESM, which are further elaborated under a series of technical guidelines. Under the Basel Convention's technical guidelines on ship dismantling, "beaching" is not accepted as impermeable floors are prescribed for full ship containment at any stage of the dismantling process. However, it is applied to relatively few end-of-life ships and is difficult to enforce in relation to most of the world's merchant fleet.

3.4 The EU Waste Shipment Regulation

The EU Waste Shipment Regulation aims to ensure the protection of the environment when waste is subject to shipment. It implements the Basel Convention at EU level, as well as the Basel "ban" by banning all exports of waste for disposal, whether hazardous or not, except to EFTA (European Free Trade Association) countries. All waste shipped between the EU and third countries as well within the EU shall be managed without endangering human health and in an environmentally sound manner throughout the period of shipment and during its recovery and disposal[6]. The requirements of the EU waste framework directive and other EU legislation,

for example, on health and safety of workers or regarding the specific management of certain materials such as asbestos shall be respected [14]. Several courts in European states (Netherlands, Belgium, Norway and France) have ruled that end-of-life ships should be considered as waste and need to be decontaminated prior to export[7].

The regulation applies to all ships which are "waste" as defined under the EU waste framework directive. In practice, however, enforcement of the regulation is difficult when a ship becomes waste outside European waters although some decisions have been made by national courts. Recent cases have shown uncertainty of some national authorities on when and how to enforce the waste shipment rules in relation to suspected end-of-life ships. The last two legal instruments are enforced to all end-of life-ships, whereas the IMO HKC covers all end-of-life, privately owned ships apart from certain small ships (< 500 GT) and excludes warships and other state-owned ships.

4. The Working Environment in Ship Recycling Facilities

Although the basis of the scrap industry was centered in Europe and U.S. during the 1970s, owing to the increased cost supporting health and safety regulations, it moved in the 1980s to the Asian region (Taiwan and South Korea). In the 1990s China, Bangladesh, India and Pakistan became the new centers of ship scrapping. More than 90% of scrapping/recycling is operated in these states mainly because it offers certain advantages to their local economies, i.e., employment and revenues [15].

However, the manner in which the ship recycling is executed, will determine the impacts of activities on

---

[6] Turkey has refused entry of the following toxic obsolete ships in its territorial waters: Olna and Olwen (2001), Sea Beirut (2002), Novocherkassk (2003) and Clemenceau (2003).

[7] It is well known that thousands of ships are built with toxic substances such as asbestos and PCBs. In the Clemenceau case, a defunct aircraft carrier laden with asbestos and PCBs was exported by the French government to India only to be called back after a French court ruled that France, in exporting the vessel, was not abiding by the rules established under the Basel Convention and Council Regulation.

the environment and worker safety and health. In case of the "beaching" technique (the common one for the Asian states), the impacts would be greater for worker injury, disease and death as well as for the local environment (contamination of water, soil, air, and other industries, i.e., fish farming). In case of piering, the impacts are negative for the environment whereas in case of dry-docking there are minimal negative environmental impacts and OHS (occupational health and safety) standards at these facilities are usually high.

The ship-breaking operations are divided into three core phases, notably preparation, deconstruction and scrap stream management [16]. In this way, it would be easier to identify all individual tasks and those related to workers' safety and health. Each phase is depended upon "safe working practices" and the flow of information with respect to physical characteristics of the ship and the dangers associated with hazardous wastes remaining on board. The "green passport" would provide some additional information on this respect. This approach is a systematic method which can be adopted to develop a safe working plan. Planning and information are important for the safe working environment of those engaged in the ship-dismantling operations. Other benefits include reductions in work-related accidents and increased productivity.

It is obvious that workers in scrapping yards are exposed to toxic fumes and excessive noise and heat, enjoy poor job security and almost a total absence of occupational safety and health regulations. Furthermore, low-paid unskilled workers are permitted to dismantle a ship and undertake the recycling operations without being prudent with regard to personal safety and protective equipment. Little attention is paid to health and safety issues and there is a lack of systematic training for such operations. As a result, deaths and injuries are very common phenomena (over the last 20 years, more than 400 workers were killed and around 6,000

sustained injuries due to gas explosions and falls of heavy iron plates) [17].

Basically, accidents originate due to absence of: (1) skills, (2) appropriate plans and working procedures, (3) precautions and personal safety equipment, (4) lack of facilities and safe working platforms/tools. Ship breaking operations expose workers to a wide range of hazards or workplace activities.

The introduction of new ship recycling techniques will assist in the safe removal, handling and disposal of hazardous and other wastes, i.e., waste pre-cleaning stations and oil reception facilities situated in close proximity to ship recycling yards could reduce the effects to personnel and the environment. The IMO has established an International Ship Recycling Fund to provide technical assistance to facilities in developing countries.

Greenpeace [18] also released a report on the economics of a system to promote clean and safe ship recycling (2005)[8]. In order to upgrade recycling facilities, the key-issues are costs and more stringent regulations but the potential trends brought exactly the opposite results , i.e., in India (Alang) it was observed that, due to stricter measures imposed on the recycling industry, some facilities are re-locating to other countries with lenient laws and thus, it resulted to job losses for nearly 3,000 direct workers and 70,000 indirect workers [19].

It is true that the recycling industry eliminates obsolete and substandard ships, and therefore it is the key element of maritime safety and environmental protection and of economic balance in the shipping markets. The more expensive it is to recycle a ship, the later it will be sent for scrap and the higher it will be the average second-hand ship's age of the world's

---

[8] India has revealed figures related to accidents and casualties for the period 1997-2000 that do not compare to figures published by Greenpeace. The AFR (accident frequency rate) based on data provided from Alang scrap-yard, assuming a working year of 2,000 hours per worker amounts to 0.96 accidents per million work hours. These numbers are considerably lower than for the ship-building and ship-repair industries.

fleet. The remaining of older ships in the market will obviously depress it but at the same time it will substantially increase the risks of loss of life and accidental pollution. This will mean even higher hazards for the maritime safety. As a result, no matter what constitute authorities and maritime industries do in order to deal with hazardous materials, the recycling procedures can better be controlled at the recycling facilities [20].

5. System Model

The key-drivers for the ship-owner's decision to send a vessel for scrap are shown below in Fig. 1 [21]. The decision criteria have been incorporated in a system dynamics model, whereby the main OHS effect of the regulatory environment (in particular the IMO new convention) with respect to adoption by recycling states are being captured.

The model distinguishes states with scrap yards in two categories: Type A states represent those which comply with the regulatory framework and apply stricter OHS rules, offering respectively lower scrap

prices; Type B states offer higher scrap prices, having lower standards of OHS.

Although a flow should exist between the two categories (i.e., Type B countries raising their OHS standards and joining Type A), this is not modeled for simplification purposes, since we are currently not examining the states' response to the draft regulation, but rather the ship-owner's choice for a recycling facility in view of the regulation (Fig 2).
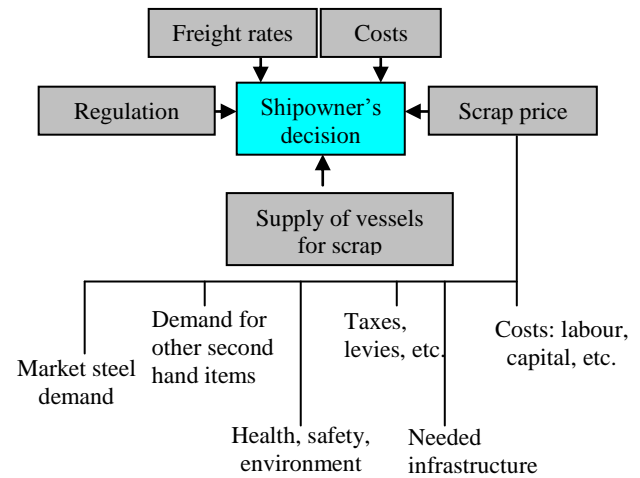

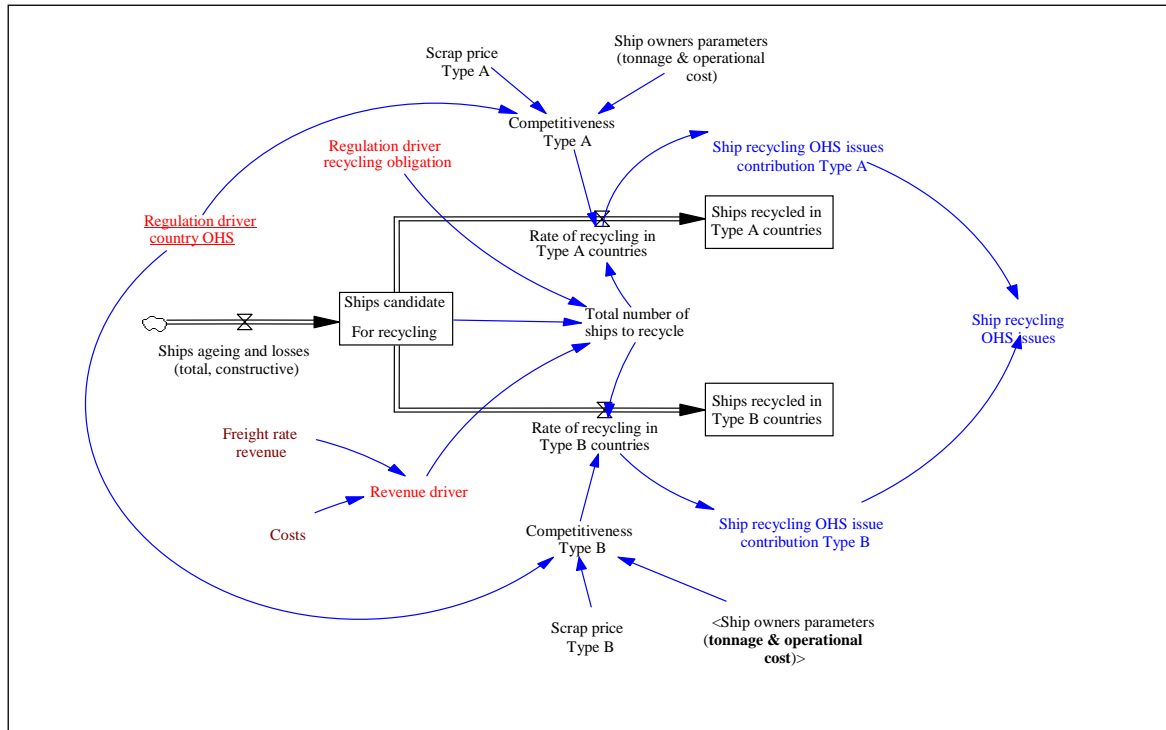**Fig. 1   Shiponwer's decision for scrap.**

Fig. 2   System model.

Table 1   Components of the model

Model element	Description
Ships recycled in Type A countries	Stock representing states which comply with the regulatory framework and apply stricter OHS rules, offering respectively lower scrap prices
Rate of recycling in Type A countries	Flow representing ship-recycling in states belonging to Type A
Rate of recycling in Type B countries	Flow representing ship-recycling in states belonging to Type B
Ships candidate for recycling	Stock expressing number of ships about to be recycled
Ships ageing and losses (total constructive)	Flow representing ships either involved in an accident and became total loss and ships reached the age-limit to send for scrap (phasing-out scheme)
Total number of ships to recycle	Simulation variable expressing the total number of ships annually to be recycled
Ship-owners parameters (tonnage and operational cost)	Parameters used to refer to decision-making criteria for sending vessels to scrap facilities
Scrap prices Types A/B	Parameters used to refer to decision-making criteria for sending vessels to scrap facilities
Competitiveness Types A/B	Auxiliary variables affecting rate of recycling
Revenue drivers (costs, freight rate revenues)	Basic parameters affecting the total number of ships being recycled
Regulation driver country OHS	Basic parameters affecting competitiveness Type A
Regulation driver recycling obligation	Basic parameters affecting competitiveness Type A
Ship recycling OHS issues	Simulation variable as derived from the ship recycling OHS issues
Ship recycling OHS issues contribution Type A	This parameter is used to define the main OHS effect of the regulatory framework by states adopting it
Ship recycling OHS issues contribution Type B	This parameter is used to define the main OHS effect of the regulatory framework by states not adopting it
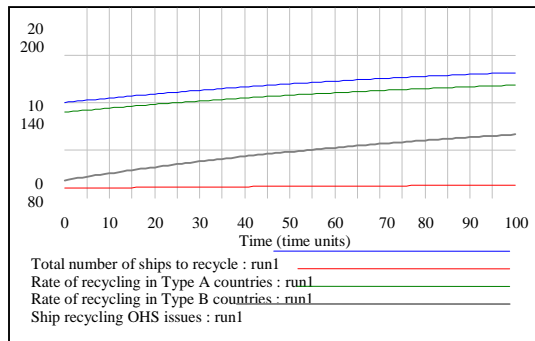
(a) Scenario
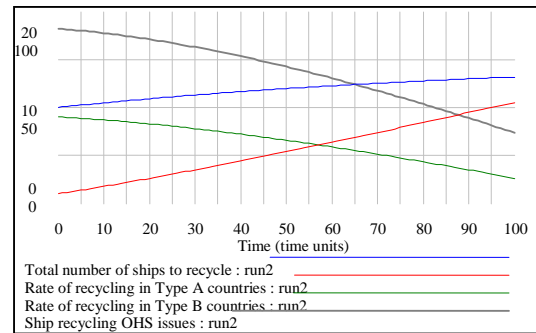
(b) Scenario

Fig. 3   Model simulation runs.

The model takes into consideration that the total number of ships to recycle is expected to increase in the near and medium term, due to ships ageing (MARPOL regulation) and accidents resulting to losses. Two scenarios were considered: (1) lack of a regulatory framework and (2) an effective regulatory framework is enforced (Fig. 3).

Scenario (1) displays that OHS conditions are deteriorating owing to the increased volume scrapped, whilst scenario (2) shows that an effective regulatory framework can lead to improved OHS conditions despite the increased volume, while the recycling facilities offer lower prices.

6. Conclusions

Scrapping of ships is one of the most difficult processes that causes impacts to human health and to the surrounding environment, but when properly planned it contributes to sustainable development. Because ships will continue to be sent for scrap since there are no alternatives, safe practices through review processes must be implemented and not only found in written documents.

An inventory of detailed international regulations and guidelines (e.g., waste management plans and assessment of risks) is imperative, along with existing

national rules referring to working conditions and environmental-friendly operations without setting the minimum requirements. This would impose certain obligations to all stakeholders involved (e.g., shipowners, shipbuilders, operators, cargo-owners, ship registers and related industries) that are not willing to pay for the safe disposal of old ships. This resembles the principles of "the polluter pays" and "end-of-life-ships" that must be adopted by the shipping industry as a whole.

As shown by the model, although the number of ships sent for scrap is expected to increase in the following years, effective regulation can contribute to the improvement of OHS conditions. If the new IMO convention is adopted by most states, it will produce harmonized rules for the recycling facilities; but the ship-owner's decision is mainly affected by fluctuations of the market. Considering the heavy criticism to the forthcoming convention, the question is to what extent it can affect the market according to its requirements.

Finally, we must note that, when the new IMO convention enters into force, it will create two major recycling markets, the first one for the convention ships and the second for non-convention ships. It would be useful to extend the model including the supply and demand dynamics of the recycling industry under the new regime.

7. Interpretation

Ship "recycling" is the terminology adopted by the IMO, though the concept is also referred to as "breaking" (ILO terminology), "dismantling" (Basel Convention terminology), and "scrapping" (joint working group of IMO/ILO/Basel Convention terminology). The term "disposal" is used to strictly address the final phase of ship recycling, whereas the term "demolition" is used referring to the process of taking a ship apart including beaching. Finally, the term "decommission" is the taking of an end-of-life ship out of service [22].

References

[1] A.B. Alexopoulos, Environmental pressures on the seafront. Safety, health and pollution issues arising from shipbreaking activities, in: Integrated Coastal Zone Management. From Theory to Co-operation for a Sustainable Future, Medsos Network, Athens, 2006.

[2] S. Dimakopoulos, The IMO's work on ship recycling, IMO News 2 (2005) 8-21.

[3] F. Bondini, P.L. Gaggero, Developments on ship recycling, in: Maritime Safety, Security and Environmental Protection, NTUA, Athens, 2007.

[4] G.P. Vlachos, The Economics and Strategy of Ship-Building, J&J Hellas Publications, Athens, Greece, 2002, pp. 497-531.

[5] CEC, Green Paper on Better Ship Dismantling, COM (2007) 269 Final, Brussels, 2007.

[6] N. Mikelis, A statistical overview of ship recycling, in: Maritime Safety, Security and Environmental Protection, NTUA, Athens, 2007.

[7] M.M. Hossain, Ship Breaking Activities and its Impact on the Coastal Zone of Chittagong, Bangladesh: Towards Sustainable Management, YPSA (Young Power in Social Action), 2007.

[8] Greenpeace, End of Life Ships, The Human Cost of Breaking Ships, FIDH report with YSPA, 2005.

[9] IMO, Guidelines on Ship Recycling, Resolution A.962(23) and Resolution A.980(24), IMO Docs, 2004.

[10] N. Mikelis, Developments and issues on recycling of ships, in: The East Asian Seas, Haikou City, 2006.

[11] ILO, Safety and Health in Ship-breaking, Guidelines for Asian Countries and Turkey, ILO Publications, 2004, pp. 55-65.

[12] IMO, Recycling of Ships. Calculating of Recycling Capacity for meeting the entry into force conditions of the HKC, MEPC 64/INF.2, 2012.

[13] UNEP, Consideration of the implementation of the Basel Convention; Technical Guidelines of the Environmentally Sound Management of the Full and Partial Dismantling of Ships, UNEP/CHW.6/23, 2002.

[14] European Commission, An Assessment of the Link Between the IMO HKC for the Safe and Environmentally Sound Recycling of Ships, the Basel Convention and the EU waste shipment regulation, Brussels, COM (2010) 88 final, 2010.

[15] A.B. Andersen, Worker safety in the ship-breaking industries, ILO issue paper (2001) 8-35.

[16] DEFRA, UK Ship Recycling Strategy, Consultation paper 2006 25-30.

[17] ILO Sectoral Activities Department, Home Page, www.ilo.org/public/english/dialogue/sector/papers/shp-break/index.htm (accessed February 11, 2009).

[18] Greenpeace, The Ship Recycling Fund: Financing Environmentally Sound Scrapping and Recycling of Sea-Going Ships, Report, 2005.

[19] J. McElroy-Brown, Shipbreaking at Alang, India. What is the right thing for this place?, TIAS 498 Independent Study, University of Washington, 2006.

[20] EC, Ship Dismantling and Pre-cleaning of Ships, Final Report, Directorate General Environment, 2007.

[21] EC, Oil Tanker Phase-out and the Ship Scrapping Industry, Report No. P59106-07, 2004.

[22] A.B. Alexopoulos，L.P. Hatzikonstantis, Occupational Health and Safety Dynamics in the Ship Recycling Industry, Unpublished report, University of the Aegean, Chios Island, 2009.

Heavy Metal Distribution in *Avicennia Marina* from Sonmiani, Pakistan Coast

Rashida Qari and Shabir Ahmed

Institute of Marine Science, Karachi 75270, Pakistan

Abstract: The accumulation of heavy metals in the *Avicennia marina* was studied in the Bhira village mangrove forest, Miani Hor Balochistan, Pakistan. Samples of leaves, stem and roots were collected randomly from the selected specie (*Avicennia marina*). The study site is receiving continuous amount of heavy metals from effluent and discharge of different sources. The concentrations of heavy metals was in decreasing order Fe > Cd > Pb > Hg in all three parts (leaves, stem and roots) of the *Avicennia marina*. The average concentration of Fe was 6.45 μg/g, Cd 0.97 μg/g, and Pb 0.71 μg/g, in mangrove plant *Avicennia marina*. The situation reflects the needs for continuous monitoring of the heavy metals in the mangrove plant forest.

Key words: Heavy metal, mangrove, accumulation, pollution, source, effluents.

1. Introduction

The dominant intertidal seed plants of the tropics and subtropics are mangroves, a general term that refers to a variety of 12 genera of halophytic shrubs and trees. Basically, a mangrove is a large woody tree like plant that has a thick and densely interwoven root network [1]

The total area covered by mangrove forests are found in Pakistan is 167,500 hectares split between the two provinces of Sindh and Balochistan. In Balochistan, mangroves are mainly found in three different patches, Miani Hor, Kalmat Hor and Gwatar bay and the total area under mangrove cover in all three sites has been estimated to be 7,340 hectares [2]. Miani Hor or Sonmiani Bay is situated at a distance of 90 km, from Karachi on the East Balochistan Coast. It comprises of three villages: viz. Dam, Sonmiani, Bhira and a settlement called Baloch Goth [3]. Miani Hor is the only area in Pakistan where three species of mangrove *Avicennia marina*, *Rhizophora mucronata* and *Ceriops tagal* occur naturally [4]. *Avicennia marina* is a shrub to medium sized tree, 2-5 meter tall

[5] this species is found from downstream to intermediate estuarine zones in all intertidal regions [6]. In Pakistan, *A. marina* is found at the mouth of rivers or in lower tidal areas [5].

The mangroves have salt exclusion or salt excretion adaptations properties, allowing survival in saline environments. Due to saline environment leaves of *A. marina* also exhibit a lot of variations. The underside of the leaves have a typical greyish-whitish colour, due to the presence of small hairs where as on surface of the leaves salt crystals are found [7]. The above ground root system of *Avicennia marina* is characterized by upright pencil like pneumatophores which originate from an underground cable root. Mangrove ecosystems are highly productive and play a vital role as a major primary producer within estuarine systems. The uniqueness of *Avicennia marina* root systems serve as habitat and nursery area for many juvenile fish and crustaceans, which have both direct and indirect socio-economic importance and are of great importance to many scientific studies. They also provide erosion mitigation and stabilization for adjacent coastal landforms [8]. In a plant-soil system, strong absorption and fixation of heavy metals by soil can easily cause residual accumulation in the

Corresponding author: Rashida Qari, professor, research fields: marine environment and marine biology. E-mail: rqari2002@yahoo.com.

soil, resulting in over-absorption of heavy metals by growing plants [9, 10].

Generally, accumulation does occur at the root level, with restricted transport to aerial portions of the plants. These indicate that plants actively avoid the uptake of trace metals. Many studies had been carried out on various mangrove plants to determine its heavy metal accumulation capability because they play an important role as a filter and natural pollution treatment centre, specialty of its root system that manage to control the water quality and trap the sediments as well as particulates which are transported by the current into the oceans from the estuaries [11-13].

In Pakistan, little is known about the specific effects and bioaccumulation of heavy metals in mangroves, although it is generally considered that mangroves show the ability to accumulate metals and possess a certain tolerance to relatively high levels of heavy metal pollution [14]. Pakistan has rich forest of mangroves that is why it was important and necessary to study the content of heavy metals accumulation in

mangrove plants.

2. Materials and Method

Three samples of mangrove tree *Avicennia marina* were collected randomly from sea to land ward in the month of November 2010 from the sampling site Bhira village, Miani Hor, Pakistan (Fig. 1). The samples were washed, dried at 60-70 $^{\circ}$C for 24 hours till a constant weight was achieved. The samples were then homogenized with a porcelain pestle and mortar to a powder form, sieved and stored in plastic bottle until further analysis. Digestion of samples was carried out as described by Denton and Burdon Jones [15]. In digested samples, concentrations of Fe, Cd and Pb and were measured by Atomic Absorption Spectrophotometer (AA-6300). Standard for calibration were prepared in deionized water from 1 mg/ml stock standard solution (May and Baker LTD Dagenham England). The values of each reported metal are the mean of three observations expressed in micro gram per gram dry weight (μg/g). For the statistical analysis, MINITAB 11.0 software was used.

Miani Hor

Legends

- Dense Mangroves
- Normal Mangroves
- Sparse Mangroves
- Natural Vegetation
- Dry Mud Flats
- Wet Mud Flats
- Sandy Area
- Saline Area
- Deep Water
- Shallow Water
- Turbid Water
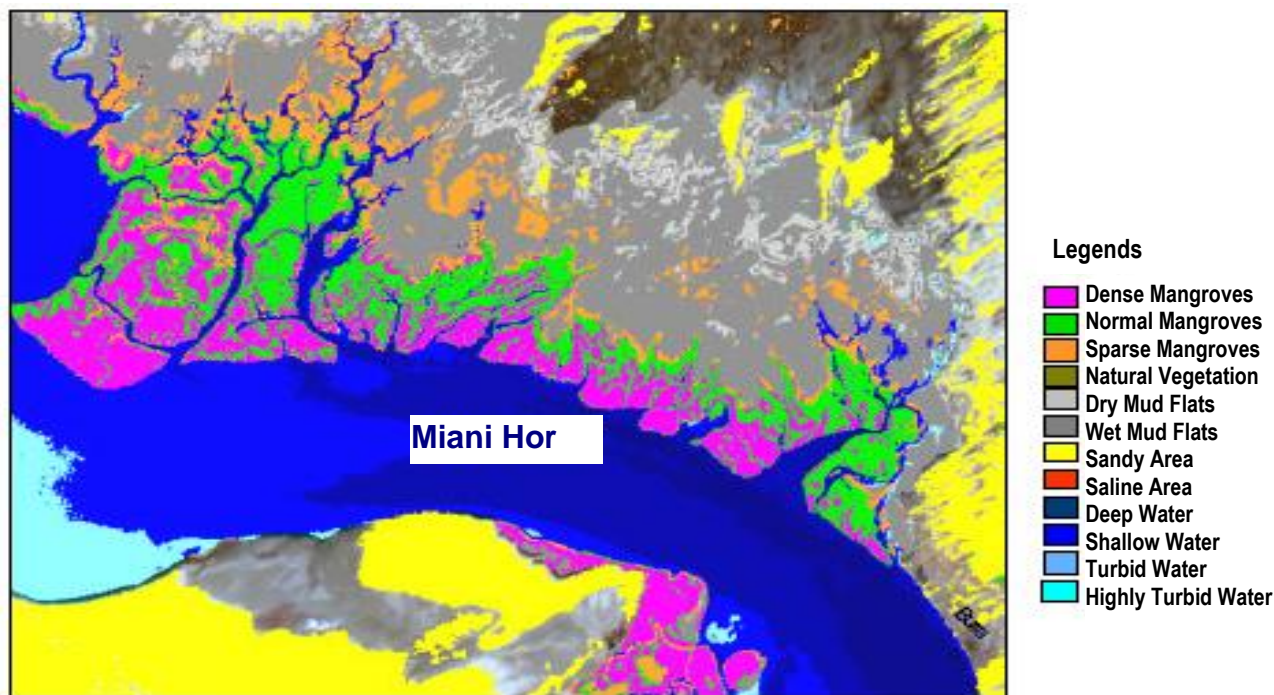- Highly Turbid Water

Fig. 1   Satellite image showing sampling site, Miani Hor [16].

3. Results and Discussion

In present work, high concentrations of heavy metal were observed at the study area of Bhira village, Miani Hor Balochistan coast and show much variation in concentration of different heavy metals (Fe, Cd, Pb, and Hg) in different parts (leaves, stem and roots) of mangrove plant *Avicennia marina*. The concentration of Fe was high as compared to other metals Cd, Pb and Hg (Fig. 2).

Fig. 2 shows that the concentration of Fe was high in roots (9.62 μg/g as compared to leaves (7.06 μg/g)

and in stem (2.64 μg/g). Similarly, the concentration of Cd was also greater in roots (2.1 μg/g) as compared to stem (0.51 μg/g) and leaves (0.31 μg/g) (Fig. 3). It is also noted that the concentration of Pb and Hg were high in roots (1.18 μg/g and 0.0018 μg/g, respectively) and lowest in stem (0.36 μg/g and 0.0017 μg/g, respectively) and leaves (0.58 μg/g and 0.0016 μg/g, respectively) (Fig. 3). The concentration of studied metals in different parts of plant in decreasing order were Fe > Cd > Pb > Hg in roots and stem, and Fe > Pb > Cd > Hg in leaves. Saenger and McConchie [17]
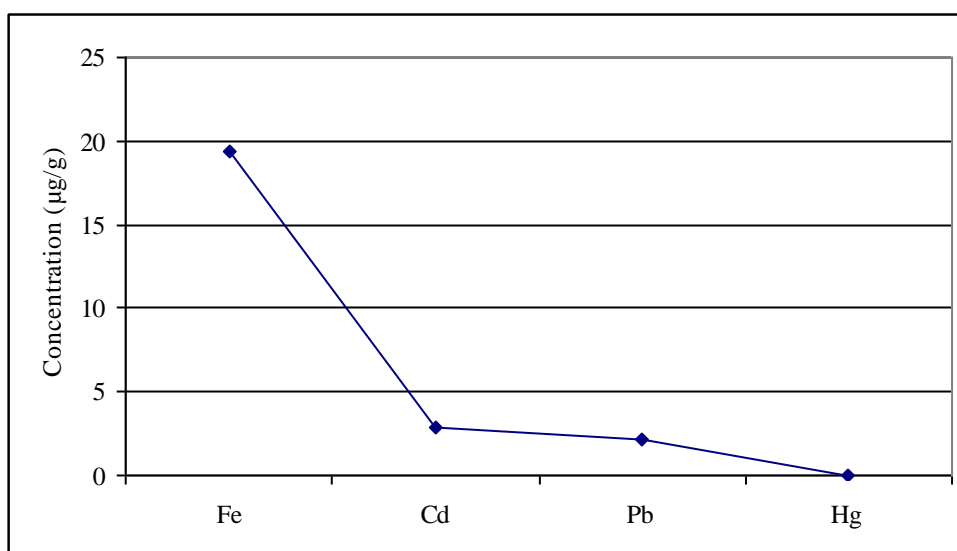

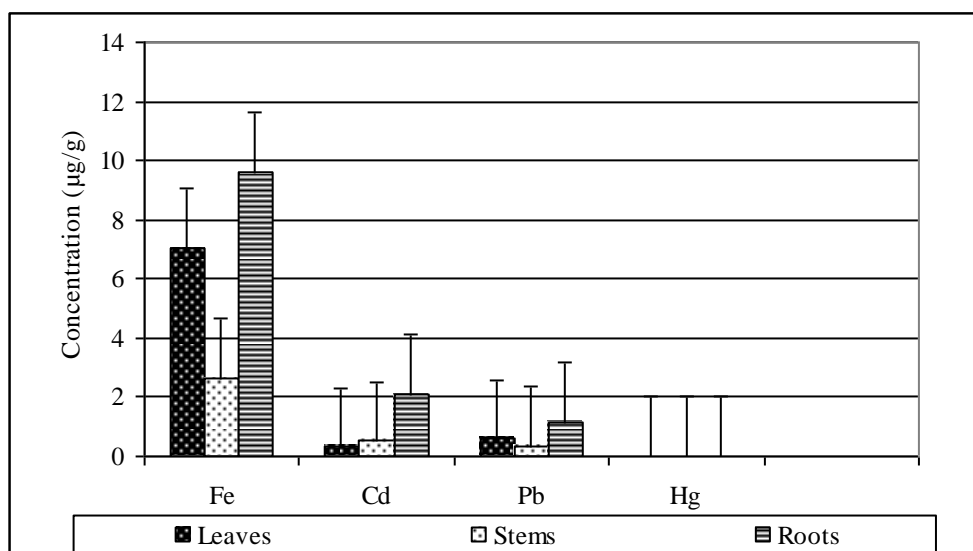**Fig. 2   Total concentration of heavy metals in *Avicennia marina*.**

Fig. 3   Heavy metal concentration in different parts of *Avicennia marina*.

reported clear tendency for Cu and Zn that are more concentrated in young leaves than in old leaves of *Avicennia marina.*

There was positive significant correlation in between studied heavy metals Fe and Cd ($r^2 = 0.712$), Fe and Pb ($r^2 = 0.916$), Cd and Pb ($r^2 = 0.934$), Cd and Hg ($r^2 = 0.912$), and Pb and Hg ($r^2 = 0.71$) found in between different parts (leaves, stem and roots) of *Avicennia marina.* The concentration distribution in plant parts like leaves, stems and roots may vary depending on the concentration of heavy metals in the sediment, the types of heavy metals and also the tolerance of the species and its parts towards the heavy metals [18, 19].

High accumulation of Fe in parts of *Avicennia marina* reveals is due to persistent break down of ships and cargo along the Gaddani ship breaking yard, some 40-46 km south from Bhira village is contributing a great contribution of Fe in ocean. Detection of other heavy metals such as Cd, Pb and Hg in the study area reflects that, vast industrialization of Windar and Hub in Balochistan, contributes a great input of cadmium and lead into the studied site, ultimately accumulated in different parts of plants in different level. Pollution of studied heavy metals from parts of the plant transfers to trophic levels via associated fauna of mangrove ecosystem i.e., fish, shrimp, crab and mud skippers etc., While effects of these pollutants on biodiversity can cause the health problems, mental deficiency, hormonal imbalances, skin erosion and mussel problems in humans when we take marine food as diet.

Therefore, present study clearly shows that concentrations of heavy metals were distributed in all parts of *Avicennia marina.* High accumulation of Fe, Cd and Pb can pose adverse effects on plant growth. In particular, stem basal diameter, leaf number and biomass production. High concentration of heavy metals accumulated in roots of *Avicennia marina* can increase the content of toxicity in plant, which causes significant degree of reduction in health and also

biodiversity of associated mangrove fauna also.

References

[1]   P.R. Pinet, An introduction to the planet Oceanus, Oceanography (1992) 427.

[2]   S.M. Saifullah, A. Rasool, Preliminary Survey of Mangroves of Balochistan, WWF-Pakistan project report, 1995.

[3]   A.A. Shah, K. Jusoff, Mangrove conservation through community participation in Pakistan: The case of Sonmiani bay, International Journal of Systems Applications, Engineering & Development 1 (4) (2007) 75-76.

[4]   F. Rasool, S. Tunio, S.A. Hasnain, E. Ahmad, Mangrove conservation along the coast of Sonmiani, Balochistan, Pakistan.Trees, 16 (2002) 213.

[5]   L. Peng, W. Xin-men, Ecological notes on the mangroves of Fujian, China, Biology and Ecology of Mangroves. H. J. Teas, (Ed.), (1983) pp. 31-36.

[6]   A.I. Robertson, D.M. Alongi, Tropical Mangrove Ecosystems, Coastal and Estuarine Series, M.J. Bowman, R.T. Barber, C.N.K. Mooers, and J.A. Raven, (Ed.), (1992) p. 329.

[7]   D.P. Gillikin, B. De Wachter, J.F. Tack, Physiological responses of two ecologically important Kenyan mangrove crabs exposed to altered salinity regimes. Journal of Experimental Marine Biology and Ecology 301 (2004) 93-109.

[8]   C. Harty, Mangrove in New South Wales and Victoria. Vista Publication, Melbourne, Victoria, 1997, p. 4.

[9]   Y. Lian, J. Xu, P. Lin, S. Meguro, S. Kawachi, Five heavy metals in propagules of ten mangrove species of China, J. Wood Sci. 45 (1999) 18-24.

[10] S. Ravikumar, G.P. Williams, S. Shanthy, N.A.A. Gracelin, S. Babu, P.S. Parimala, Effect of heavy metals (Hg and Zn) on the growth and phosphate solubilising activity in halophilic phosphobacteria isolated from Manakudi mangrove, J. Environ. Biol. 28 (2007) 109-114.

[11] K.F. Yu, B.S. Kamber, M.G. Lawrence, A. Greig, J.X. Zhao, High precision analysis on annual variation of heavy metals, lead isotopes and rare earth elements in mangrove tree rings by inductively coupled plasma mass spectrometry, Nucl. Instr. and Meth. In Phys. Res. 255 (2007) 99-408.

[12] C.A.R. Silva, A.P. de Silva, S.R. Oliveira, Concentration, stock and transport rate of heavy metals in a tropical red mangrove, Natal, Brazil, Mar. Chem. 99 (2006) 2-11.

[13] M.W. Clark, D. McConchie, D. W. Lewis, P. Saenger, Redox stratification and heavy metal partitioning in Avicennia-dominated mangrove sediments: A geochemical

model, Chemical Geology 149 (1998) 47-171.

[14] B.Y. Kamaruzzamam, M.C. Ong, K.C.A. Jalal, S. Shahbudin, O.M. Nor, Accumulation of lead and copper in Rhizophora apiculata from Setiu mangrove forest, Terengganu, Malaysia, Journal of Enviro. Bio. 3 (2009) 821-824.

[15] R.W. Denton, Burdon-Jones, Trace metal in algae from the Great Barrier Reef., Mar. Pollut. Bull. 17 (1986) 98-107.

[16] T. Qureshi, Mangroves of Pakistan: Status and Management. IUCN (2005).

[17] A. J. Baker, P. I. Walker, Ecophysiology of Metal Uptake by Tolerant Plants, Heavy Metal Tolerance in Plants: Evolutionary Aspects, A. J. Shaw, (Ed.), 1990, pp. 155-178.

[18] L. De Lacerda, J. Abrao, Heavy metal accumulation by mangrove and salt marsh intertidal sediments, Mar. Pollut. Bull. 17 (1986) 246-250.

[19] P. Saenger, McConchie, Heavy metals in mangroves: methodology, monitoring and management ePublications@SCU Research and Scholarly Publication Southern Cross University (2004).

Tsunami Hazard Assessment in the Alboran Sea for the Western Coast of Algeria

Lubna A. Amir

Faculty of Earth Sciences, University of Sciences and Technology Houari Boumedienne, Algiers 16111, Algeria

Abstract: In October 1790, a destructive earthquake occurred near Oran city in the western part of Algeria (MSK, Medvdev-Sponheuer-Karnik macroseismic intensity: X). It generated a tsunami that inundated the Spanish and North Africa coasts. The regional tectonic includes NW-SE compressional stress in Algeria and NE-SW strike-slip structures in the Alboran basin. In this work, we identified tsunami sources for the Alboran from numerical modeling. The sea bottom displacement is calculated from the Okada equations. The tsunami's propagation is simulated with the SWAN code. The identified tsunami source for the 1790 event is a 7.5 magnitude earthquake at the entrance of the Oran harbor, with a pure reverse faulting, probably associated with the Murdjajo fold. The tsunami wave height profile that is obtained for the city of Oran showed an initial withdrawal of the sea that was followed by tsunami waves reaching 2 meters in height. The results obtained in Spain agree with the observations reported in the literature. Finally, the simulations led to a better understanding of the interdisciplinary approach to be considered as for tsunami sources in the Alboran. Sedimentary mass-movements should be now included as an additional component in the tsunami hazard assessment for the West Mediterranean. The contribution of sedimentary disturbance due to the series of canyons offshore the western margin could induce water waves higher than 2 meters in Western Algeria.

Key words: Alboran, tsunami, modelling, sedimentary mass-movements, earthquake, Western Algeria.

1. Introduction

Northern Algeria is located at the boundary between the African and European plates. Although the convergence rate between those tectonic plates is in the range of order of 4-7 mm per year, the compressive motion results in the occurrence of tsunamigenic earthquakes in Western Mediterranean. In particular, the Alboran Sea separates the Ibero area in Spain from the Maghreb in Morocco and Western part of Algeria.

Table 1 lists the major tsunamis reported for the Ibero-Maghreb region. The events are from the Spanish tsunami catalog which can be downloaded at http://www.fomento.es.

In Table 1, three events are identified in the Alboran Sea. The first one reported dates back to 1790, by the time of the Spanish domination in Northern

Africa. This event has been reported and documented by the Spanish [1]. The second event listed in Table 1 dates back to 1804. It corresponds to the transition between the Spain and French Domination in North Africa. We have no historical reports that document with a series of details on the effect of this tsunami. Therefore, it is very hard to constrain the source from that event. The latest dates back to 1954. This tsunami observed and reported in the coast of Spain corresponds to the effect of a very destructive earthquake inland (M=6.7) that hit Orleansville [2].

The Orléansville city which has been destroyed by the 6.7 magnitude in 1954 has been rebuilt and re-named El Asnam. In October 1980, El Asnam was the location of another destructive earthquake (M=7.3) that generated a tsunami observed once again in the Spanish coasts. Previous papers attempted to model a landslide-generating tsunami for that event [3].

The scope of this paper is (1) to constrain the source location of the 1790 Alboran tsunami from numerical simulation and (2) to review distinct tsunami scenario.

Corresponding author: Lubna A. Amir, Ph.D., research fields: natural hazard, earthquakes and tsunami mitigation. E-mail: lamir@usthb.dz.

Table 1   Tsunami events in the Ibero-Maghreb (Spanish tsunami catalog available at : http://www.fomento.es)

Year	Source location	Year	Source location
-218	Cádiz	1856 (08.21)	Algeria
-210	Cádiz	1856 (08.22)	Algeria
-60	SW Portugal	1885	Algeria
881	Cádiz	1891	Algeria
1706	Canary Islands	1954	Alborán Sea
1755 (11.01)	SW Portugal	1969	Gorringe Bank
1755 (11.02)	SW Portugal	1975	AGFZ (Acores Gibraltar Fault)
1755 (11.16)	Coruña	1978	Cádiz
1756	Baleares	1980	Algeria
1790	Alborán Sea	2003 (05.21)	Algeria
1804	Alborán Sea	2003 (05.27)	Algeria

In this work, we discuss the impact of landslides process on tsunami hazard modeling in the Alboran region.

The paper is organized in three main sections. The section Methodology (Section 2) presents all the documents, data and principle of the tsunami modeling used to propose scenarios for tsunami hazard assessment in the Western Algeria. The section Results (Section 3) reports the computed scenario for an earthquake and for mass-movements tsunami that is the most appropriate regarding documentation and geological setting of the Alboran. Finally, the last section discusses and concludes on the results obtained as for the tsunami hazard in western part of Algeria.

2. Methodology

2.1 Historical Documents: The 1790 Alboran Tsunami

In October 1790, a devastating earthquake hit Oran city in North Western of Algeria (Io = IX-X, MSK Scale). Historical spanish documents reports that two thousand people died in North Africa [1]. The seismic crisis consisted of a series of foreshocks reported during September and beginning of October 1790. The main shock occurred at 01:15 AM on the 9th of October and aftershocks are reported until February 1790. The earthquake was felt as far as 200 km from Oran to Almeria and Carthagena in southern Spain.

A tsunami was generated just a few minutes after the main shock. This tsunami occurred during the Spanish domination in North Africa while vessels and marine traffic were very important between the 2 continents. In the Algerian coast, the sea withdrawal was about 200 meters. In Spain, the sea penetrated inland by 50 meters nearby Almeria. In the harbour of Carthagena, the ship "Marie- Salope-la Chata" broke its moorings and the sea rose by 1.8 meters [1].

Because of lack of information, the 1790 Oran earthquake is poorly constrained. As regards the importance of damages, the epicenter was suggested to be located inland [1]. But a suggestion to re-evaluate it offshore was as well discussed since a tsunami was reported.

2.2 Geological and Geophysical Framework

The Alboran Sea is narrow and located between the African and Eurasian convergent tectonic plates (< 1 cm·yr^{-1}). It is surrounded by the Betic and the Rif Cordilleras and connects the West offshore Mediterranean to the Iberian Peninsula. The geological structure of the region is complex [4, 5].

The orogeny of the Tell Atlas was favored by the convergence between the tectonic plates. It lays in a SW-NE direction along the whole Mediterranean coast. The associated neogene active faults are reverse, transverse or normal. Strike-slip structures are as well to be quoted since they can displace sedimentary mass and induce slide-components to potential generated

tsunamis. Locations of seismological events and first attempts to model tsunami brought out the tsunamigenic potential for identified lineaments.

In the nearby of Oran, an active thrust fault related to the Murdjajo Anticline was identified from field investigations in the Oranie area [6]. The Murdjajo anticline is a N050 assymetric geological structure of about 32 km in length. These evidences for active thrust faulting lead the scientific community to expect that the 1790 earthquake might be associated to the Murdjajo tectonic structures with an epicenter supposed to be located inland as well. Geological field and historical investigations revealed the total length of the reverse fault is about 60 km and the fault dips at 60° to the NW. The seismicity recorded in the Ibero-Maghreb area is mostly associated to strike-slip and thrust mechanisms. In the Tell Atlas, the seismicity is shallow. A strong earthquake in the Oranie region may come from accidents dipping 40° to 60° in the NW direction [6].

Offshore geophysical surveys reveal thrust active fault along the margin and numerous strike-slip accidents that mark the Alboran Ridge. Potential destructive active fault are identified in Iberia and in North Africa. In the South East of Spain, the existence of a NE-SW offshore continuation of the Carboneras active strike-slip fault system was reported in Ref. [5]. They suggested it may generate a potential destructive 7.2 magnitude (Mw) earthquake. The West Mediterranean Margin is also marked by a series of escarpment with active fault such as the Arzew fault and escarpment in the northwest of Algeria. Finally, the Arzew escarpment and the related active fault (offshore Western Algeria) were well imaged from swath bathymetry [7, 8]. This structure could be as well a candidate for a destructive earthquake triggering water waves.

2.3 The Tsunami Hazard Modeling

The modeling is performed with the SWAN code [9]. This program is a shallow water model that solves the 2D-non linear Eulerian equations with a finite difference scheme.

$$\frac{\partial U_x}{\partial t} + U_x \frac{\partial U_x}{\partial x} + U_y \frac{\partial U_x}{\partial x} + g \frac{\partial H}{\partial x}$$
$$= F U_y$$
$$+ F^{(x)} - g \frac{U_x (U_x^2 + U_y^2)^{1/2}}{C^2 (D + H - R)} \quad (1)$$

$$\frac{\partial U_y}{\partial t} + U_x \frac{\partial U_y}{\partial x} + U_y \frac{\partial U_y}{\partial y} + g \frac{\partial H}{\partial y}$$
$$= - F U_x$$
$$+ F^{(y)} - g \frac{U_y (U_x^2 + U_y^2)^{1/2}}{C^2 (D + H - R)} \quad (2)$$

$$\frac{\partial H}{\partial t} + \frac{\partial (D + H - R) U_x}{\partial x} + \frac{\partial (D + H - R) U_y}{\partial y} - \frac{\partial R}{\partial t}$$
$$= 0 \quad (3)$$

With: U_x = velocity in the X-direction; U_y = Velocity in the Y-direction; g = gravity acceleration; t = time; H = Water height above the sea level; R = Sea bottom motion; F = Coriolis parameter; C = Chezy coefficient; D = depth; $F^{(x)}$ and $F^{(y)}$ = functions for the meteorological effect.

All simulations are computed with the ETOPO 1 minute global relief database [10]. The grid extends from 34°N to 42°N and 6°W to 2°E.

The sea bottom motion due to the earthquake is calculated from the Okada analytic equations [11] within the topographic grid. The Kanamori law links the seismic moment Mo to the moment magnitude Mw [12]. Empirical seismological relationships [13] help to evaluate the geometry of the fault plane (length and width). The resolution grid for the earthquake and tsunami modelling is 1,853 meters in the (Ox) and (Oy) direction. In this work, we suggest the 1790 earthquake epicenter is located offshore the Oran bay. The tsunami scenario parameters are selected as regards to the important damage reported [1], the tectonic sketch of the Alboran and the Tell Atlas [4, 7] and the field investigations carried out on the Murdjajo related fold [6]. Different tests are computed with a pure thrust fault mechanism (rake is 90°) and earthquake moment magnitudes varying from 7 to 7.5. Fault strike ranges between 40° to 65° NE-SW. The location of the epicenter was also tested

along the Oran and Arzew bays. The dips tested are between 20 ° to 45 ° and the focal depths vary from 5 km to 15 km.

Landslide sources are very difficult to examine since it is impossible to predict with accuracy the path of the sediments' motion and turbidity currents. Morphometric parameters to constrain the potential slides are crucial to select areas where landslide hazard can be identified [14].

Although the process is complex, the swan code can be used to simulate the main sea bottom motion parameters (sedimentary volume displaced and velocity). In particular, this was applied to the study of the 1994 Skagway tsunami [9]. Here, the morphometric parameters for the Western Algeria are estimated from slope gradients varying between 15 to 35 ° and a sedimentary velocity of 20 m/s. The tested scenarios focused on the Oran-Arzew-Mostaganem region where hydrodynamic processes related to the Cheliff, the Macta and the Magoun rivers and mass movements triggered by the earthquake shaking are hard to distinguish [15]. In addition, inspired from the limits of landslide sources triggering tsunami modeling from the 1994 Skagway study [9], we also considered simplified models to evaluate maximum landslide hazard scenario (Mostaganem, Arzew and

Oran). Catastrophic scenarios for tsunami hazard from mass movements in the Alboran are displayed in Fig. 1. These are related to the North African coastal submarine canyons. Tests for single slides and a combination of slides along the margin were carried out.

3. Results

3.1 The 1790 Alboran Tsunami

While testing the different ruptures' model for the tsunami source, the more the strike and the dip are, the greater the South East Spanish coast is affected. Consequently, the choice of the strike and the dip parameters helped to constrain the seismic source.

From the results obtained, the best scenario is a 7.5 magnitude (Mw) earthquake with a pure thrust mechanism at the entrance of Oran harbor. The fault strike is 65 °N and the dip is 45 °SE. The focal depth is 5 km. The length and width of the fault is 73.3 km by 29.2 km. The calculated corresponding slip is 3.45 meters.

The simulation shows that tsunami water waves in the Oran, Arzew and Almeria Bay are trapped along the coasts for a long time. The tsunami propagation in the Alboran Sea lasts about an hour (Fig. 2).
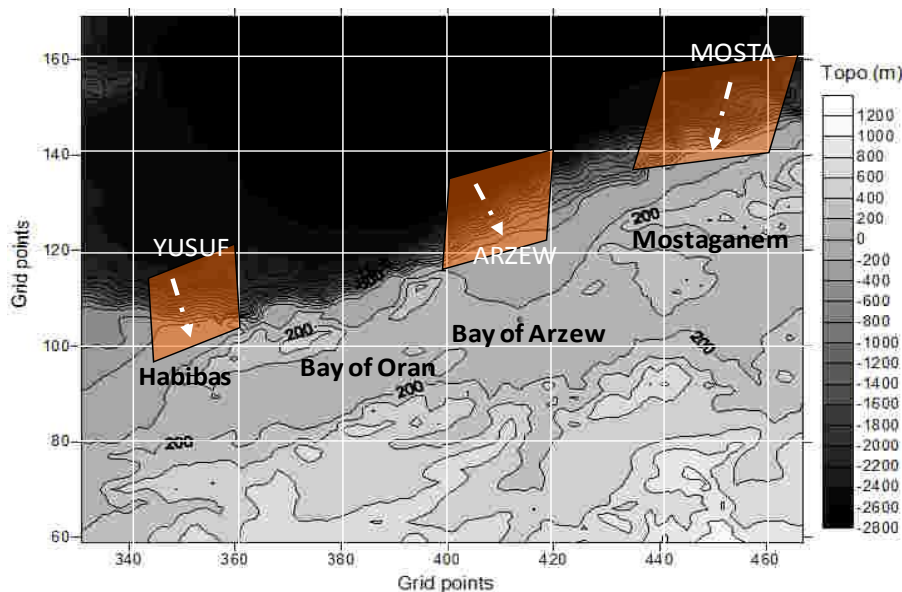

Fig. 1   Location of slide scenarios for landslide-triggering tsunami in Western Algeria.

The tsunami waves reach the Spanish coasts from less than 20 minutes after the earthquake onset. The Almeria gulf is the first affected by the waves. The Balearic Islands are also affected by the tsunami waves from 40 minutes. The tsunami wave propagated after 04 min from the onset of the earthquake is displayed in Fig. 2a. The sea movements simulated for a time period of 50 minutes are shown in Fig. 2b.

The water height profile computed are represented in Fig. 3 for Oran (0.4 ° W, 35.9 ° N) and Fig. 4 for Carthagena. The maximum water height calculated for Oran is about 2 meters for a point of interest located at a water depth of 15 meters near the harbor. For Carthagena, a value of 1.5 meters is estimated for a point of interest located at a water depth of 6 meters

near the coastal city. In Oran, the first crest is rapidly followed by a trough of 2 meters. Then, the results show the sea level disturbance with several waves of 1 meter in height. In Carthagena, the first crest appears 20 meters later. It is followed by a trough of 1 meter and water waves ranging between 0.5 meter and 1 meter in height.

3.2 The Mass Movements Scenario

Water flow energy and debris transported are among the potential sources of impact along the shoreline. The reference to test valid scenario on coastal mass movements are the details described as for the vessels damage in 1790 [1] and potential risk due to the oil marine traffic in industrial harbor [15].
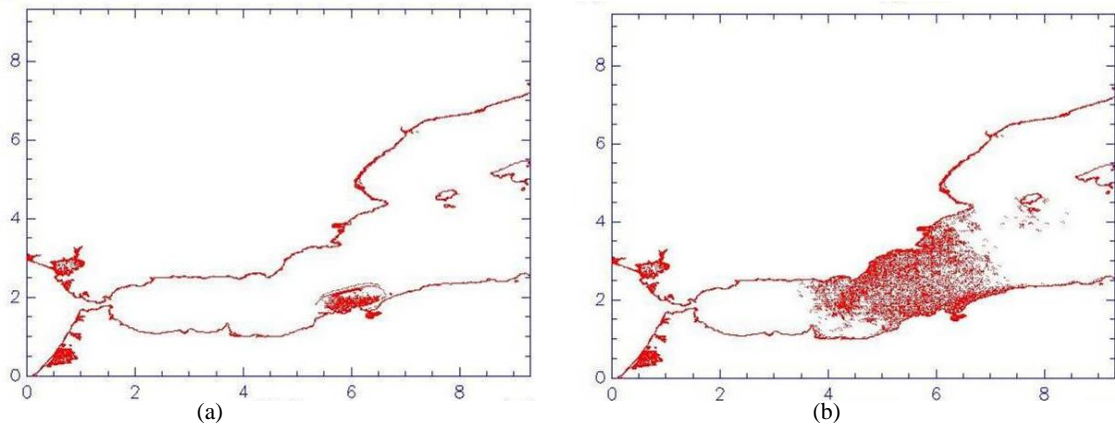

(a)   (b)

Fig. 2   Snapshots for the tsunami propagation in the Alboran, Mw = 7.5, Strike = 65 ° N, Dip = 45 ° SE. (a) : waves propagation after 04 minutes, (b): waves propagation after 50 minutes. The bottom and the left axes represent the X and Y coordinates respectively (m).
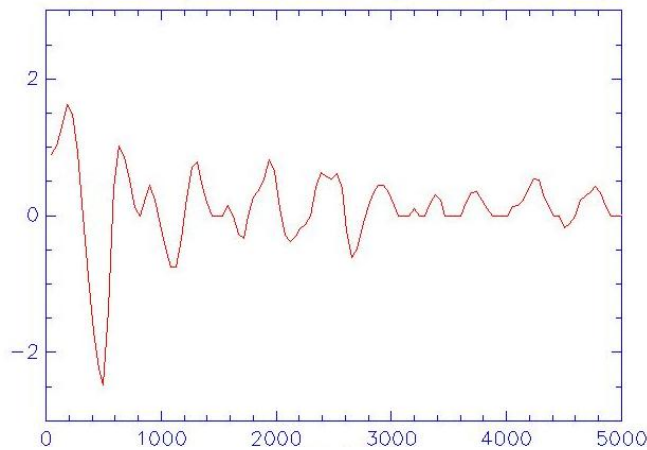

Fig. 3   Water wave profile computed in Oran (0.4° W, 35.9° N) with the swan code [6]. The left axis represent the water height (m). The bottom axis shows the time (s). This point is located at a water depth of 15 meters.
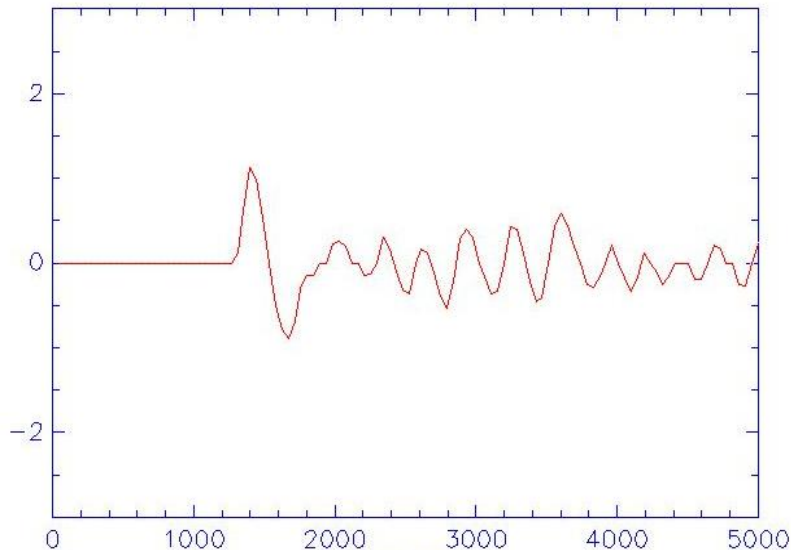
Fig. 4   Water wave profile computed in Carthagena (0.98° W, 37.58° N) with the swan code [9]. The left axis represent the water height. It is expressed in meters. The bottom axis shows the time. It is expressed in seconds. This point is located at a water depth of 6 meters.

At first, the scenarios tested from the morphometric parameters reveal that the energy to induce a killer wave is not enough. On the other hand, the tsunamis triggered by the 1954 and 1980 earthquakes in El Asnam were minor [3].

The results obtained also show that a sedimentary displacement of 3 meters is necessary to produce significant destructive waves in North Africa (Oran) (Fig. 5) and South of Spain (Carthagena) (Fig. 6). The results plotted in both figures correspond to mass-movements scenarios. The red curve represent the combination of mass-movements in the nearby of
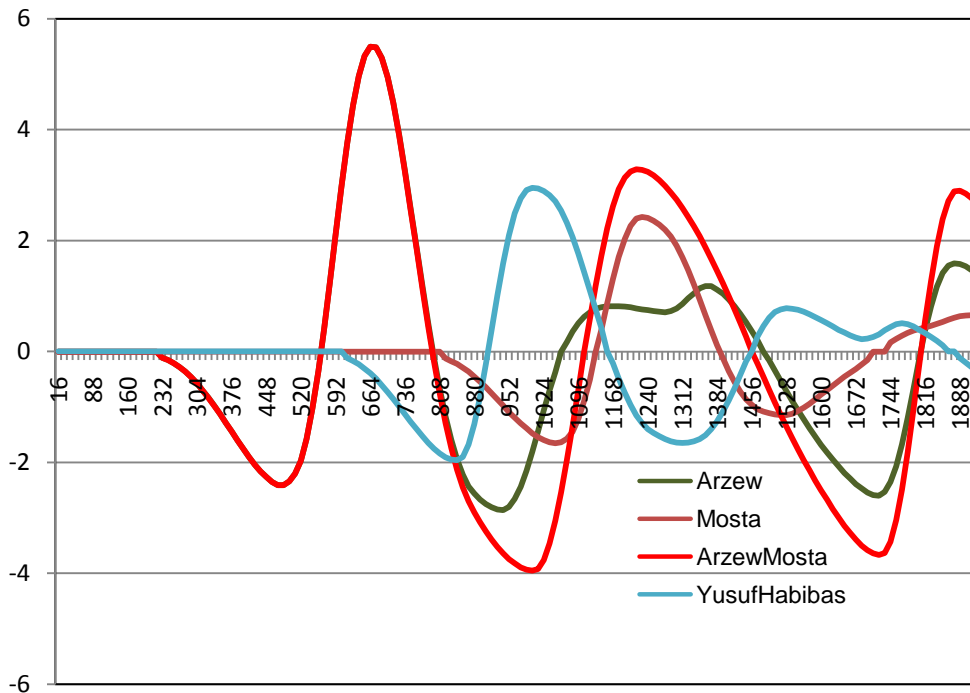

Fig. 5   Water wave profile computed in Oran with the swan code [9]. The left axis represent the water height (m). The time (bottom axis) is in seconds. This point is located at a water depth of 6 meters.
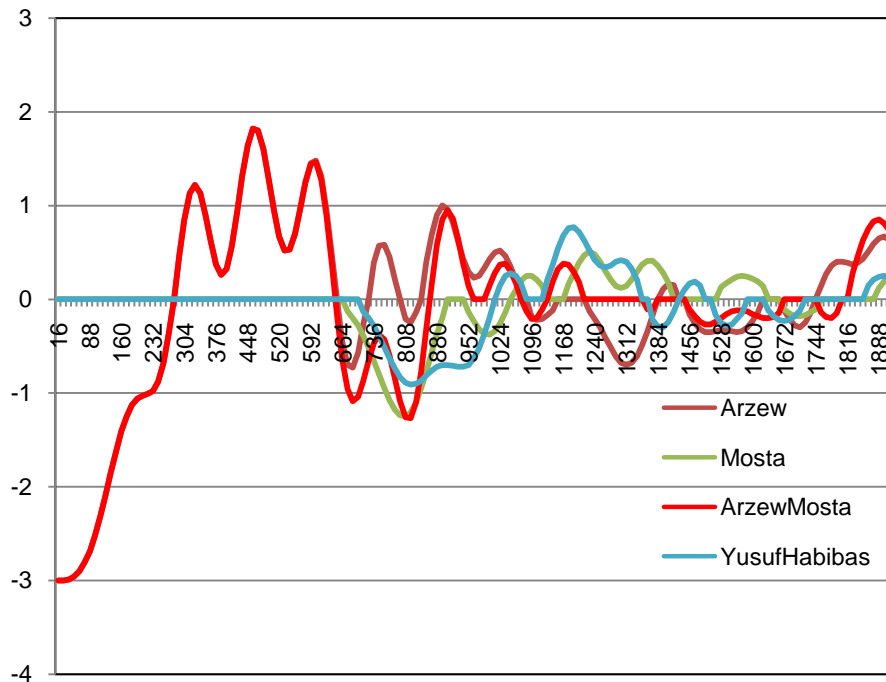
Fig. 6 Water wave profile computed in Carthagena with the swan code [9]. The left axis represent the water height (m). The time (bottom axis) is in seconds. This point is located at a water depth of 6 meters.

Mostaganemen and in the Arzew bay. The brown, green and blue curves correspond to single mass-movements in Mostaganem, in the Arzew bay and near the Habibas Islands respectively. The maximum water wave height computed is 6 meters for Oran (Fig. 5) and 1.7 meters for Carthagena (Fig. 6).

4. Discussion and Conclusions

From tsunami hazard modeling, this study suggests that the 1790 Alboran Tsunami Source could be a 7.5 (Mw) magnitude earthquake with a thrust active fault marked by a strike of $65\,°N$ and dipping $45\,°SE$. The epicenter is located offshore at the entrance of the Oran Harbour. The fault length is 73 km and its width is 29 km. The numerical results agree with the historical observations reported in Ref. [1].

This fault model corresponds to the global trend offshore the Algerian Margin. In 2003, a magnitude Mw=6.8 earthquake in Boumerdes-Zemmouri triggered a tsunami in the West Mediterranean [16, 17]. The Spanish tide gauge in the Balearic recorded run-ups around 2 meters to 3 meters in height. Several fault models were proposed for the 2003 tsunami

source to fit the wave amplitude recorded by the tide gauges [18, 14]. Hence, we found the resulting fault strike and dip and the focal depth for the tsunami induced by the 2003 Zemmouri earthquake are in the range of order of the 1790 Alboran tsunami source.

Offshore Geophysical surveys confirmed the existence of such active thrust fault in the Algerian Margin [7, 8, 20]. Moreover, swath bathymetry and seismic surveys in the West Mediterranean highlighted evidences of turbidites currents and imaged headwall scarp on submarine canyons suggesting slides and debris flow probably associated to earthquakes events [4, 8, 21].

Nevertheless, these sources parameters are for an earthquake rupture's scenario and consider a single fault segment. The focal depth could be re-adjusted to 7 km and the magnitude reduced to 7.2 when considering the impact of generated mass-movements. Therefore, maximum sedimentary mass displacement scenarios were introduced in the tsunami modelling to analyze along the coast the sedimentary disturbance contribution to water height profile computed for the same points of interests (i.e., Oran for Algeria and

Carthagena for Spain). The results obtained revealed that only combined mass motions scenario and topography explain significant water height along the Algerian and the Spanish coasts. Consequently, it is very difficult to simulate with accuracy a landslide source generating a tsunami in the Mediterranean exactly as how it was hard to explain the Dockslide Model for the 1994 Skagway Tsunami [9].

Finally, all numerical simulations were carried out with the ETOPO 1 minute NGDC database [10]. The descriptions provided in historical documents for the tsunami effect on the North Africa and Spanish documents are poor. For these reasons, improvements on the modelling (finer grid resolution for the coastal areas, multiple fault rupture's model ...) are necessary to define the 1790 Alboran tsunami. However, the present work and paper helped to provide a preliminary review of the potential candidates for tsunami hazard in the Alboran.

Acknowledgements

References

[1]   J.M. Lopez Marinas, R. Salord, El periodo sismico oranes de 1790 a la luz de la documentación de los archivos españoles (M.S. Boughacha, Trans.) (in Spanish), I.G.N. Publication, Madrid, 1990.

[2]   B.C Heezen, M. Ewing, Orleansville earthquake and turbidity currents, AAPG Bull. 39 (1955) 2505-2514.

[3]   J. Roger, H. Hébert, J-C Ruegg, P. Briole, The El Asnam 1980 October inland earthquake: A new hypothesis of tsunami generation, Geophys. J. Int., DOI: 10.1111/j.1365-246X.2011.05003.x., Published Online: April 14, 2011, http://onlinelibrary.wiley.com/enhanced/doi/10.1365-246X.2011.05003.x/.

[4]   A. Ammar, A. Mauffret, C. Gorini, H. Jabour, The tectonic structure of the Alboran Margin of Morroco, Revista de la Sociedad Geologica de Espana 20 (2007) 247-271.

[5]   E. Gracia et al., Active faulting offshore SE Spain (Alboran Sea): Implications for earthquake hazard assessment in the Southern Iberian Margin, Earth and Planetary Science Letters 241 (2006) 734-749.

[6]   Y. Bouhadad, The Murdjajo, Western Algeria, fault-related fold: Implications for seismic hazard, Journal of Seismology 5 (2001) 541-558.

[7]   A. Mauffret, Northwestern (Maghreb) Boundary of the Nubia (Africa) plate, Tectonophysics 429 (2007) 21-44.

[8]   A. Domzig, V. Gaullier, P. Giresse, H. Pauc, J. Deverchere, K. Yelles, Deposition processes from echo-character mapping along the Western Algerian margin (Oran-Tenes), Western Mediterranean, Marine and Petroleum Geology 26 (2009) 673-694.

[9]   C. L. Mader, Numerical Modeling of Water Waves, Second Edition, CRC Press, Boca Raton, 2004, p. 269.

[10] C. Amante, B. W., Eakins, ETOPO 1 Arc-Minute Global Relief Model: Procedures, Data Sources and Analysis, NOAA Technical Memorandum NESDIS NGDC–24, 2009.

[11] Y. Okada, Internal deformation due to shear and tensile faults in a half-space, Bulletin of seismological society of America 82 (1992) 1018-1040.

[12] H. Kanamori, D. Anderson, Theoretical basis of some empirical relations in seismology, Bulletin of seismological society of America 65 (1975) 1073-1095.

[13] D. L. Wells, K. J. Coppersmith, New empirical relationships among magnitude, rupture length, rupture width, rupture area, and surface displacement, Bulletin of seismological society of America 84 (1994) 974-1002.

[14] B. G. McAdoo, Mapping submarine landslides, in: Marine and Coastal Geographic Information Systems, Peter Fisher, Taylor and Francis, (Ed.), London, 1999, Chapter 14.

[15] L. Amir, A. Cisternas, W. Dudley, B. McAdoo, Coastal impact of tsunami in industrial harbors: Study case of the Arzew-Mostaganem region (Western Coast of Algeria, North Africa), in: Proceeding of the 3rd Speciality Conference on Disaster Prevention and Mitigation, Montreal, Quebec, May 29-June 1, 2013.

[16] A. Bounif et al., The 21 May 2003 Zemmouri (Algeria) earthquake Mw 6.8: Relocation and afterschock sequence analysis, Geophysical Research Letters, DOI:10.1029/2004GL020586, Published Online: Oct. 8, 2004,http://onlinelibrary.wiley.com/enhanced/doi/10.1029/2004GL020586/.

[17] P.-J. Alasset, H. Hebert, S. Maouche, V. Calbini, M. Meghraoui, The tsunami induced by the 2003 Zemmouri

earthquake (Mw=6.9): Modelling and results, Geophysical Journal International 166 (2006) 213-226.

[18] X. Wang, P. L. F. Liu, A numerical investigation of Boumerdes-Zemmouri (Algeria) earthquake and tsunami, Comp. Model. Eng. Sci. 10 (2005) 7-184.

[19] A. Sahal, J. Roger, S. Allgeyer, B. Lemaire, H. Hebert, F. Schnidele, F. Lavigne, The tsunami triggered by the 21 May 2003 Boumerdes–Zemmouri (Algeria) earthquake: field investigations on the French Mediterranean coast and tsunami modelling, Nat. Hazards Earth Syst. Sci. 9 (2009) 1823-1834.

[20] J. Deverchere et al., Active offshore Boumerdes, Algeria, and its relation to the 2003 May Mw 639 earthquake, Geophysical Research Letters, DOI:10.1029/2004GL021646, Published Online: Feb. 23 2005, http://onlinelibrary.wiley.com/doi/10.1029/2004GL021646/pdf.

[21] G. Lastras, M. Canals, R. Urgeles, J.E. Hughes-Clarke, J. Acosta, Shallow slides and pockmarck swarms in the Eivissa Channel, western Mediterranean sea, Sedimentology 51 (2004) 1-14.

Editor's Acknowledgement

All manuscripts submitted to Journal of Shipping and Ocean Engineering are usually reviewed by at least one member of the editorial board members. This commits them to up to 12 assessments each year and the Editor thanks them for so generously giving their time and advice. The Editor is also grateful to many other assessors who have helped in 2013.

At the same time, every manuscript submitted to Journal of Shipping and Ocean Engineering is refereed by at least 2 outside experts in the field. The Editor and the Editorial Executive Committee gratefully acknowledge the considerable time and help the reviewers who gave during 2013. The Editor thanks very much for their advice and for their promptness in dealing with the manuscripts.

The Editor also thanks for the understanding, support and help from our authors, readers and other people and agencies.

Call for Papers

Description

Journal of Shipping and Ocean Engineering is an international, scholarly and peer-reviewed journal (print and online) published monthly by David Publishing Company, USA which was founded in 2001. The journal publishes research results and academic papers on ocean science, shipbuilding industry, Marine equipment technology, ocean exploitation and nuclear power applications, which aims to promote international academic exchanges and push the ocean science and technology to develop.

The journal is published in English. The e-journal provides free and open access to all of its content on our website. Accepted papers will immediately appear online followed by printed in hard copy.

Information for Authors

1. The manuscript should be original, and has not been published previously. Do not submit material that is currently being considered by another journal.

2. Manuscripts may be 4000-15000 words or longer if approved by the editor, including an abstract, texts, tables, footnotes, appendixes, and references. The title should be on page 1 and not exceed 15 words, and should be followed by an abstract of 100-200 words. 3-5 keywords or key phrases are required.

3. The manuscript should be in MS Word format, submitted as an email attachment to our email address.

4. Authors of the articles being accepted are required to sign up the Transfer of Copyright Agreement form.

5. Authors will receive 2 hard copies of the journal containing their articles.

Peer Review Policy

Journal of Shipping and Ocean Engineering is a refereed journal. All research articles in this journal undergo rigorous peer review, based on initial editor screening and anonymous refereeing by at least two anonymous referees.

Editorial Procedures

All papers considered appropriate for this journal are reviewed anonymously by at least two outside reviewers. The review process usually takes two to three weeks. Papers are accepted for publication subject to no substantive, stylistic editing. The Editor reserves the right to make any necessary changes in the papers, or request the author to do so, or reject the paper submitted. A copy of the edited paper along with the first proofs will be sent to the author for proofreading. They should be corrected and returned to the Editor within seven days. Once the final version of the paper has been accepted, authors are requested not to make further changes to the text.

Submission of Manuscript

All manuscripts submitted will be considered for publication. Manuscripts should be sent online or as an email attachment to: shipping@davidpublishing.org**.**

Welcome to visit our website at: http://www.davidpublishing.org.